EFFECTIVENESS OF DIAGONAL OPENING REINFORCEMENT IN REINFORCED CONCRETE CHIMNEYS UNDER GRAVITY AND LATERAL SERVICE LOADS

by

Dovlet Akyniyazov

B.S., Civil Engineering, Middle East Technical University, 2014

Submitted to the Institute for Graduate Studies in
Science and Engineering in partial fulfillment of
the requirements for the degree of
Master of Science

Graduate Program in Civil Engineering

Boğaziçi University

2016

EFFECTIVENESS OF DIAGONAL OPENING REINFORCEMENT IN REINFORCED CONCRETE CHIMNEYS UNDER GRAVITY AND LATERAL SERVICE LOADS

APPROVED BY:

Assist. Prof. Sami And Kılıç (Thesis Supervisor)	.....
Assoc. Prof. Kutay Orakçal	.....
Assoc. Prof. Vail Karakale (Marmara Univ.)	.....

DATE OF APPROVAL: 28.07.2016

ACKNOWLEDGEMENTS

My genuine regards are to my thesis supervisor Assist. Prof. Sami And Kılıç for his guidance and support throughout my study. His valuable knowledge and experience made it possible to write this thesis report.

I also want to thank Kutay Orakçal and Vail Karakale for their comments and reviews about my thesis study.

I would like to thank Selçuk Altay, who was helpful in writing my thesis report.

I aknowledge my gratitude to TUBITAK (The Scientific and Technological Research Council of Turkey) for their financial support in my graduate study and writing my thesis report.

I am grateful to the former CICIND Secretary Klaus Kaemmer and members of the CICIND Governing Body for their support in decision and writing of my thesis study. The alternative opening corner reinforcement design configuration in terms of horizontal and vertical rebars was originally suggested as a study topic by the CICIND President Michael Angelides, who is gratefully acknowledged.

Last but not least, I want to thank my beloved parents, grandparent, my brother and sisters for their love, continuous support, which made it possible for me to follow a graduate degree.

ABSTRACT

EFFECTIVENESS OF DIAGONAL OPENING REINFORCEMENT IN REINFORCED CONCRETE CHIMNEYS UNDER GRAVITY AND LATERAL SERVICE LOADS

Diagonal rebars are traditionally placed at the corners of openings in reinforced concrete chimneys in order to prevent crack formations. However, the sloping rebars pose a difficulty in the slipform construction process since they cross the vertical lines of operation of the hydraulic lifting system. This study investigates design alternatives in terms of the reinforcement configurations that may be used instead of the diagonal corner rebars. A tall reinforced concrete chimney was modeled using hexahedral finite elements for the windshield and line elements for all reinforcing steel rebars. The hexahedral elements enabled the insertion of reinforcing steel rebars into the windshield wall thickness. The vertical, hoop and additional opening reinforcements were included in the model explicitly. The lap splicing and staggered configurations of the vertical reinforcements were taken into account. Nonlinear constitutive material models were used for the windshield concrete and reinforcing steel rebars. Winfrith concrete material model was used to model the behavir of windshield concrete. Plastic kinematic material model was used to model the behavior of reinforcement. The response of the chimney under gravity and lateral service loads was investigated. The nonlinear response of the chimney was solved dynamically for the applied loads, removing the necessity of iterations that are typically used in nonlinear static analysis approaches. Crack widths and patterns around the opening, stresses at the opening region and in the corner reinforcements obtained from simulations were reported. In lights of the findings of the study, suggestions were made in terms of design alternatives for opening corner reinforcements.

ÖZET

BETONARME BACALARDA DİYAGONAL KÖŞE DONATISININ DİKEY VE YANAL YÜKLER ALTINDAKİ ETKİNLİĞİ

Diyagonal çelik donatılar, çatlak oluşmasını önlemek amacıyla geleneksel olarak betonarme baca açıklıklarının köşelerine yerleştirilir. Diğer taraftan, eğri çelik donatılar hidrolik kaldıraç sisteminin dikey sınırlarını geçtiği için kayar-kalıp inşaat süreci için zorluk arz eder. Bu çalışma, donatı konfigürasyonu bakımından diyagonal çelik donatılar yerine kullanılabilecek alternatif tasarımları araştırır. Uzun betonarme baca modelini oluşturmak için bacanın beton kalıbı altı yüzeyli sonlu elemanlar, bütün donatılar ise kiriş elemanlar olarak modellendi. Altı yüzeyli elemanlar, donatıların duvar kalınlığındaki beton kalıbın içine yerleştirilmesine olanak sağladı. Dikey, çember ve açıklık donatıları modele doğrudan dâhil edildi. Dikey donatıların bölüm etaplı ve aşamalı konfigürasyonu hesaba katıldı. Baca kalıp betonu ve donatılar için doğrusal olmayan bileşen malzeme modelleri kullanıldı. Baca kalıp betonunun özelliklerini modellemek için Winfrith beton malzeme modeli kullanıldı. Donatıların özelliklerini modellemek için plastik kinematik malzeme modeli kullanıldı. Bacanın, yanal yükleri altında ve yerçekimine verdiği tepki araştırıldı. Genelde doğrusal olmayan statik analiz yaklaşımlarında kullanılan tekrarlama gereğini ortadan kaldırarak, bacanın doğrusal olmayan tepkileri uygulanan yükler için dinamik olarak çözüldü. Açıklık etrafındaki çatlak genişliği ve düzeni ile açıklık bölgesinde ve köşe donatılarda simülasyonlardan elde edilen basınç sonuçları rapor edildi. Araştırmanın bulguları ışığında, açıklık köşe donatıları için alternatif tasarımlar açısından çeşitli öneriler öne sürüldü.

TABLE OF CONTENTS

ACKNOWLEDGEMENTS iii
ABSTRACT iv
ÖZET v
LIST OF FIGURES viii
LIST OF TABLES xii
LIST OF SYMBOLS xiii
LIST OF ACRONYMS/ABBREVIATIONS xv
1. INTRODUCTION 1
1.1. Overview 1
1.2. Importance of the Research Project 1
1.3. Aim of the Research Project 2
1.4. Outline 2
2. LITERATURE SURVEY 4
2.1. Design Codes on RC Chimneys 4
2.2. Design Codes on RC Structures other than Chimneys 6
2.3. Literature Review on Published Journals 7
3. DESCRIPTION OF THE RC CHIMNEY 10
3.1. Chimney Geometry 10
3.2. Chimney Openings 11
3.3. Chimney Windshield Reinforcement 12
3.4. Chimney Opening Reinforcement 14
3.5. Other Structural Components 15
4. SELECTION OF THE NUMERICAL METHOD 16
4.1. Solution Procedure 16
4.2. Finite Element Formulations 17
4.3. Contact Mechanism 18
4.4. Concrete Material Model 18
4.4.1. Ottosen Failure Surface 18
4.4.2. Concrete Model under Tension 19

4.4.3. Concrete Model under Compression 20
4.4.4. Concrete Model under Shear 21
4.5. Reinforcement Material Model 23
4.6. Brick Liner and Corbel Ring Material Models 24
5. FE MODELING OF THE RC CHIMNEY 25
5.1. Mesh Resolution of the FE Model 25
5.2. FE Model of the Chimney 25F-5 27
5.3. FE Model of the Diagonal Corner Reinforcement 31
5.4. FE Model of the Vertical and Horizontal Corner Reinforcement 32
5.5. Boundary Conditions of the Chimney 25F-5 33
5.6. Loading Conditions of the Chimney 25F-5 34
6. SIMULATION RESULTS UNDER GRAVITY SERVICE LOADS 35
6.1. Validation of the FE Model 35
6.2. Comparison of Design Alternatives under Gravity Service Loads 41
7. SIMULATION RESULTS UNDER LATERAL SERVICE LOADS 47
7.1. Loading Period of the Simulations 47
7.2. Comparison of Design Alternatives under Lateral Service Loads 50
8. CONCLUSIONS AND FUTURE WORK 56
8.1. Conclusions 56
8.2. Future Work 58
REFERENCES 59

LIST OF FIGURES

Figure 3.1. Vertical profile of the chimney 25F-5. 11

Figure 3.2. Opening details of the chimney 25F-5. 12

Figure 3.3. Inner and outer vertical reinforcement distributions of the chimney 25F-5. 13

Figure 3.4. Opening reinforcement details of the chimney 25F-5. 14

Figure 3.5. Brick liner and corbel ring details of the chimney 25F-5. 15

Figure 4.1. Crack width and behavior of Winfrith concrete under tension. . . 20

Figure 4.2. Behavior of Winfrith concrete under compression. 21

Figure 4.3. Behavior of Winfrith concrete under shear. 22

Figure 4.4. Stress-strain relationship for reinforcement material model. 23

Figure 5.1. Mesh resolution and node sharing of finite elements; (a) Model 1, (b) Model 2. 26

Figure 5.2. Layout of vertical reinforcements of the cross section "A-A" for the high-resolution Model 1 and medium-resolution Model 2. 27

Figure 5.3. FE model of the chimney 25F-5. 29

Figure 5.4. FE model of the vertical and hoop reinforcements. 30

Figure 5.5. FE model of the brick liner and corbel rings. 31

Figure 5.6. FE model of the diagonal opening corner reinforcements. 32

Figure 5.7. FE model of the vertical and horizontal opening corner reinforcements. 33

Figure 5.8. FE model of the boundary conditions in chimney 25F-5. 33

Figure 5.9. Lateral service loads. 34

Figure 6.1. Evolution of energies for Model 1 under gravity service loads. . . . 36

Figure 6.2. Evolution of energies for Model 2 under gravity service loads. . . . 36

Figure 6.3. Total weight of the chimney 25F-5 for Model 1. 38

Figure 6.4. Total weight of the chimney 25F-5 for Model 2. 38

Figure 6.5. Top vertical displacement time history for Model 1. 39

Figure 6.6. Top vertical displacement time history for Model 2. 39

Figure 6.7. Mode shapes of 25F-5, (a) 1st mode, T1 = 1.65 *sec*, (b) 2nd mode, T2 = 1.61 *sec*. 41

Figure 6.8. Contours of minimum principal stresses for Case 1 under gravity service loads. 42

Figure 6.9. Contours of minimum principal stresses for Case 2 under gravity service loads. 42

Figure 6.10. Deformed shape of the opening region under gravity service loads for both Cases 1 and 2; displacements are magnified 1000 times for illustration purposes. 44

Figure 6.11. Contours of axial stresses at the diagonal corner reinforcements under gravity service loads. 45

Figure 6.12. Contours of axial stresses at the vertical and horizontal corner reinforcements under gravity service loads. 45

Figure 7.1. Resonance in structural dynamics [32]. 48

Figure 7.2. Evolution of energies under lateral service loads. 49

Figure 7.3. Push-over curve of the chimney 25F-5. 49

Figure 7.4. Evolution of base moment under lateral service loads. 50

Figure 7.5. Contours of minimum principal stresses for Case 1 under lateral service loads. 51

Figure 7.6. Contours of minimum principal stresses for Case 1 under lateral service loads. 51

Figure 7.7. Crack formations around the opening region for Case 1 under lateral service loads. 53

Figure 7.8. Crack formations around the opening region for Case 2 under lateral service loads. 53

Figure 7.9. Contours of axial stresses at the diagonal corner reinforcements under lateral service loads. 54

Figure 7.10. Contours of axial stresses at the vertical and horizontal corner reinforcements under lateral service loads. 54

LIST OF TABLES

Table 3.1. Vertical profile of the chimney 25F-5. 10

Table 3.2. Parameters of the openings in chimney 25F-5. 12

Table 3.3. Inner hoop reinforcement distribution in chimney 25F-5. 13

Table 3.4. Outer hoop reinforcement distribution in chimney 25F-5. 14

Table 6.1. Simulation run-times for Models 1 and 2. 35

Table 6.2. Weights of the structural components of the chimney 25F-5. 37

Table 6.3. Modal periods of the chimney 25F-5. 40

Table 6.4. Stress values at the corner reinforcements under gravity service loads. 46

Table 7.1. Stress values at the corner reinforcements under lateral service loads. 55

LIST OF SYMBOLS

a	Aggregate Diameter
A, B, λ	Ottosen Failure Surface Constants
A_s	Steel Area
$B-300$	25 Mpa-concrete class
cm	Centimeter
deg	Angular Degree
D	Dynamic Magnification Factor
f_c	Compressive Strength of Concrete
f_u	Ultimate Strength of Reinforcing Steel
f_y	Yield Strength of Reinforcing Steel
GB	Gigabyte
GPa	Gigapaskal
I_1	First Stress Invariant
J_2	Second Deviatoric Stress Invariant
kg	Kilogram
KJ	Kilojoule
kN	Kilonewton
l	Opening Width
L	Length
$\left[M\right]$	Mass Matrix
m	Meter
mm	Millimeter
MJ	Megajoule
MN	Meganewton
MPa	Megapaskal
p	Material Mass Density
sec	Second
t	Chimney Wall Thickness

$\ddot{u}_n$	Acceleration
w	Crack Width
β	Frequency Ratio
ϕ	Rebar Diameter
σ_1, σ_2, σ_3	Principal Stresses
σ_y	Yield Stress

LIST OF ACRONYMS/ABBREVIATIONS

3D	Three Dimensional
ACI	American Concrete Institute
ASCE	American Society of Civil Engineers
CICIND	Internation Committee for Industrial Chimneys
FE	Finite Element
RC	Reinforced Concrete
SSC	Shear Stress Reduction Coefficient

1. INTRODUCTION

1.1. Overview

Industrial chimneys are tall and slender structures which are used to discharge hot flue gases at higher elevation to the atmosphere. They are commonly referred to as flue gas stacks and are generally located adjacent to a steam-generating boiler and the gases are carried to them with ductwork. Reinforced concrete (RC) chimneys are generally designed to withstand gravity, wind, temperature and earthquake loads. Breach openings are located in chimneys where ductwork exists. Openings are critical zones in reinforced concrete chimneys, because concrete area is lost due to presence of openings in chimney windshield. Therefore, special provisions are required in opening regions in order to prevent brittle failure and crack formations. Design codes provide different reinforcement schemes for the opening regions. The common ground of additional opening reinforcements is to place horizontal and vertical rebars at the lintels and sides of the opening, respectively. In addition, few codes have requirements to place diagonal rebars at the corners of the opening regions in order to prevent diagonal crack formations under lateral and gravity service loads.

1.2. Importance of the Research Project

There exist inconsistency among codes regarding the additional opening reinforcement requirements in RC chimneys. ASCE 7-10 and CICIND codes do not require placement of diagonal reinforcements at the corners of the opening in RC chimneys. However, ACI 307 code requires diagonal reinforcements to be placed at the corners of the opening. Commentary of ACI 307 does not provide any confirmation about the background information on the diagonal corner reinforcement provisions. Research studies are required to understand the necessity of diagonal opening reinforcement in RC chimneys.

1.3. Aim of the Research Project

RC chimneys are continuous, tapered cantilever structures in nature. Slipforming construction method is used to provide continuous form and to avoid any discontinuities in RC chimneys. Due to tapered geometry, slipform construction provides good opportunity to adjust the diameter and thickness of the windshield concrete changing along the height of the chimney. Slipform must not be stopped at any elevation during the construction of chimneys due to the fact that cold joints con occur when slipforming stops. In terms of the construction practice, opening diagonal rebars are difficult to place in the concrete chimney windshield, considering that reinforced concrete chimneys are erected using climbing formworks.

The requirement to place the diagonal rebars at the corners of the opening is not related to strucutral capacity and internal stresses. It is purely related to the construction method, and intended to be effective under everyday service loads. The aim of this study is to investigate whether additional vertical and horizontal corner rebars can be as effective as the diagonal corner rebars placed at the corners of openings in terms of preventing diagonal cracks and stress distributions around the opening region under lateral and gravity service loads. A full 3D finite element (FE) model was constructed by including explicitly all horizontal, vertical, and diagonal rebars. The concrete windshield was modeled with volumetric finite elements and all reinforcing rebars were modeled with line finite elements.

The results of the alternative configuration of opening corner reinforcements and traditional diagonal reinforcements were compared. In light of the findings of the study, suggestions were made in terms of design alternatives for opening corner reinforcements.

1.4. Outline

This report presents the full numerical investigation of diagonal opening reinforcements in RC chimneys. Chapter 1 presents the current construction practice and the importance of the research project.

Chapter 2 provides code provisions and previous work done on the effectiveness of diagonal opening reinforcements in RC structures.

In chapter 3, geometric and reinforcement properties of a 115 m RC chimney, which is selected as a case study for this research project, is provided.

Chapter 4 includes the numerical method used in FE analyses. Constitutive material models, finite element formulations, and contact mechanism used in the analyses are presented.

In chapter 5, finite element techniques used to model the RC chimney is encompassed. A full 3D FE model was generated to carry out the simulations under lateral and gravity service loads. Mesh resolution of the chimney 25F-5 also included in this chapter.

Chapter 6 gives the validation of the FE model by means of energy evolution, total wieght and total vertical displacement of the chimney. Results of the fine-mesh and medium-mesh resolution models were compared. Moreover, the response of the chimney under gravity service loads and the stress-strain distribution patterns are presented in this chapter.

Chapter 7 provides the numerical analyses results for two different corner reinforcement configurations under lateral service loads. Comparison between the effectiveness of the diagonal opening corner reinforcements and vertical and horizontal opening corner reinforcements were made in terms of the observed crack widths and patterns at the opening region, and stress distributions around the opening and corner reinforcements under lateral service loads.

Finally, chapter 8 concludes the thesis report and provides code recommendations based on the results of the FE analyses. Moreover, future work recommandations are presented to fully understand the effectiveness of diagonal corner reinforcements in RC chimneys under strong ground motions.

2. LITERATURE SURVEY

2.1. Design Codes on RC Chimneys

This chapter investigates the opening corner reinforcement requirements and design provisions for RC structures. Openings are mainly present in RC deep beams, slabs, shear walls and chimneys. Current code provisions, previous researches and conducted tests are summarized and discussed in the following sections. This study intends to identify the effectiveness of the diagonal rebars placed at the corners of the openings in RC chimneys. Related to the detailing of the reinforcements around the openings of RC chimneys, different design codes provide similar provisions in general but there are slight distinctions in between. This section presents a comparison of design criteria embodied in ASCE 7-10, ACI 307 and CICIND codes related to the additional opening reinforcements in RC chimneys. The intention was to extract the related information from the codes and to summarize the provisions. Similarities and differences between the requirements of the design codes were discussed.

ASCE 7-10 [1] section 15.6.2 describes the additional reinforcement requirements for the opening regions of RC chimneys. According to ASCE 7-10, regions with large openings, where cross-sectional area loss is greater than 10%, shall be designed and detailed for vertical force, shear force and bending moment demands along the vertical direction with an over-strength factor of 1.5. This requirement applies for the region above and below the large opening(s) by a distance equal to half of the width of the largest opening in this region. Appropriate reinforcement development lengths shall also be provided beyond the required region of over-strength. It should be noticed that in ASCE 7-10, reinforcement orientation around the openings is not restricted. The provision only requires the opening region be strong enough "over-strength factor shall be at least 1.5" to resist any force demand. This could be achieved by providing additional reinforcement in the region by adding vertical and horizontal reinforcements. However, ASCE 7-10 does not necessitate explicit usage of diagonal reinforcements at the corners of the opening regions.

In Model Code for Concrete Chimneys document CICIND [2], section 10.3 provides the reinforcement requirements around the opening regions. It is stated that the minimum vertical reinforcement ratio should be 0.0075 in a distance of half the width of the opening on each side of the opening. However, no specific information is provided for the amount of additional horizontal reinforcement in the opening region. Both horizontal and vertical additional reinforcements around the openings should extend beyond the edge of the opening by at least half the width of the opening plus the bond length of the bars.

Sections 4.4.5-4.4.9 of ACI 307-08 [3] provide provisions for the additional reinforcement detailing around the openings of RC chimneys. In addition to the reinforcement determined by design, the ACI 307-08 code requires to place additional reinforcement as close to the opening as proper spacing of bars will permit by extending the reinforcement past the opening a minimum of the development length. According to ACI 307-08, at each side of the opening, the additional vertical reinforcement shall have an area at least equal to the design steel ratio times one-half the area of the opening. At both the top and bottom of each opening, additional reinforcement shall be placed having an area at least equal to one-half the established design circumferential reinforcement interrupted by the opening. Unless otherwise determined by a detailed analysis, the area A_s of this additional steel at the top and at the bottom shall not be less than that given by Equation 2.1.

$$A_s = \frac{0.06 f_c t l}{f_y} \tag{2.1}$$

where f_c is the specified compressive strength of concrete in MPa, t is the concrete thickness at opening in mm, l is the width of opening in concrete chimney shell in mm and f_y is the specified yield strength of reinforcing steel in MPa.

ACI 307-08 states that for openings larger than 600 mm wide, diagonal reinforcing bars with a total cross-sectional area, in square millimeters, of not less than 2.54 of the shell thickness, in mm, shall be placed at each corner of the opening. For openings 600 mm wide or smaller, a minimum of two 16 mm reinforcing bars shall be placed diagonally at each corner of the opening. However, the amount appears to be in mm^2 of not less than 5.08 of the wall thickness in mm in ACI 307-95 [4] and ACI 307-98 [5]. In ACI 505-53 [6] and ACI 505-54 [7], diagonal reinforcement at the corners of the opening shall have a combined cross-sectional area in square millimeters of not less than 2.54 of the shell thickness in mm, regardless of the opening size. Commentary of ACI 307-08 does not provide any information about the background information on the diagonal reinforcement provisions. Additionally, there are no limitations in regarding to the relative spacing between successive diagonal corner rebars.

In the literature, the first mention of diagonal rebar placement at the corners of the openings was found in the paper entitled "Design of Reinforced Concrete Chimneys" by Mingle published in 1918 [8]. Mingle proposed the vertical rebars be bent into the sides with a gradual bend to accommodate the corners of the opening. He also suggested at least three extra vertical rebars of the same size as the others be bent and placed on each side of the opening. "They keep the corners of the opening from cracking on a line parallel to the diagonal" was the argument behind placing the diagonal reinforcements at the corners of the opening. In ACI 307-08, additional diagonal reinforcement requirement is given in section 4.4.8. Code requires additional diagonal bars at the corners of the opening to be placed, instead of bending vertical bars as provided by Mingle.

2.2. Design Codes on RC Structures other than Chimneys

Reinforced concrete chimneys are tapered conical wall structures in nature. There are other RC structural members which can be acknowledged as comparable to chimneys, such as structural shear walls, deep beams, reinforced concrete slabs.

Codes require additional reinforcements around wall openings. In the ACI 318-11 [9] code, in section 14.3.7, in addition to the minimum reinforcement required by 14.3.1, not less than two No. 16 bars in walls having two layers of reinforcement in both directions and one No. 16 bar in walls having single layer of reinforcement in both directions shall be provided around window, door, and similar sized openings. Such bars shall be extended to develop f_y in tension at the corners of the openings.

In the U.K. Standard Method of Detailing Structural Concrete [10], section 6.5.2 provides reinforcement design requirements for openings in walls. Isolated openings which are smaller than the spacing of the reinforcement need not be trimmed. Where an opening does affect the structural integrity, consideration should be given to the use of diagonal rebars at the corners of the opening, to provide better crack control. Where an opening occurs in a wall which does not affect the structural integrity, it should be trimmed with bars of diameter one size larger than that used in the surrounding wall. For such situations the minimum wall thickness should be increased to 175 mm.

In the U.K. Standard Method of Detailing Structural Concrete, section 6.2.2 provides reinforcement design requirements for openings in slabs. For large isolated openings with sides 500 – 1000 mm, affected rebars should be displaced equally either side of the opening or cut or slide back to face of opening. Compensating rebars of equal area should be provided to trim all sides. Trimmers should extend a minimum 45ϕ (nominal anchorage length) beyond the opening. If the slab depth exceeds 250 mm, diagonal reinforcement of similar area should be provided at the top and bottom corners of the opening, where practical.

2.3. Literature Review on Published Journals

There exists several publishes journals and conference proceedings on the effectiveness and functionality of the diagonal reinforcements placed at the corners of the openings in RC slabs, deep beams and shear walls.

In addition to the aforementioned design codes, which provide minimum requirements to design a structure, there are several scientific articles in the literature on the diagonal reinforcement provisions around openings. Lin and Kuo [11] studied finite element analysis and experimental work to observe the ultimate strength of shear wall with opening under lateral load. Test results of specimens R3, R4 and R5, which were fabricated with same size of opening but different reinforcing patterns around opening, were compared. Specimen with diagonal reinforcement has a 15% reduction in strength while a 25% reduction in strength was observed for specimen with vertical and horizontal reinforcement. In addition to that, smaller distortion around opening was observed for specimen with diagonal reinforcement. Test results indicated that the reinforcement around opening highly affected the ductility and shear strength of the wall with opening. The shear capacity contributed by the diagonal reinforcements reached 40% of its yield strength, however the shear capacity contributed by the vertical and horizontal reinforcement reached only 20% of its yield strength.

In the Concrete International magazine [12], corner bars are defined as opening bars placed on a diagonal at each corner. Although they are not explicitly required, it is good practice to use them—they provide more efficient restraint against cracks at the re-entrant corners.

Daniel *et al.* [13] conducted experiments to understand the effects of openings on structural walls under reversing loads. They observed that there was no yielding of reinforcement in the lintels even after the vertical wall reinforcement yielded. The short lintels effectively coupled the wall piers without the use of special diagonal reinforcement.

Boon *et al.* [14] studied the structural performance of one-way reinforced concrete slabs with rectangular opening. Most effective detailing to increase the flexural capacity of reinforced concrete slabs with openings is by providing additional rectangular reinforcement around the opening. Moreover, it has been observed that the effect of additional diagonal bars was not significant.

Mansur *et al.* [15] studied reinforced concrete beams with large rectangular openings that are subjected to bending and shear. The conclusion drawn from experimental investigation was that diagonal bars for corner reinforcement are more effective in controlling crack width and reducing beam deflection.

Conclusion can be made that horizontal and vertical reinforcements placed at the corners of the opening in RC slabs, deep beams and shear walls are as effective as the diagonal reinforcements. However, there does not exist any research projects and published articles on the diagonal opening reinforcements in RC chimneys. They are being places as a method of construction since the early years of RC chimneys.

3. DESCRIPTION OF THE RC CHIMNEY

115 m tall chimney 25F-5 located in Tupraş Refinery was selected as a case study for the thesis study. A rectangular opening cut of 50 degrees existed at one third of the height of the chimney above the pile cap. The chimney is of interest to the research project since diagonal rebars were used at the four corners of its opening. The chimney was designed according to the ACI 307-69 [16] code. Earthquake loads governed the capacity requirements of the chimney 25F-5. Therefore, it was designed and constructed to widthstand the earthquake loads. Wind and gravity service loads were not the major loading conditions for the chimney 25F-5. However, it collapsed during the 1999 Izmit earthquake at the region where opening existed. The collapse of the chimney was previously investigated by Kilic *et al.* [17].

3.1. Chimney Geometry

Chimney 25F-5 had a conical tapered shape with varying outer and inner slopes at different elevations. Table 3.1 provides the outside slope, outer diameter and shell thickness values of the chimney 25F-5 along the height.

Table 3.1. Vertical profile of the chimney 25F-5.

Height (m)	**Outside Slope** (%)	**Outer Diameter** (m)	**Wall Thickness** (m)
115	1	6.60	0.20
90	1	7.10	0.22
60	1.5	8.00	0.28
40	1.75	8.70	0.30
0	2	10.30	0.45

Total height of the chimney 25F-5 was 115 m above the pile cap. Large rectangular opening existed at the elevation of 1/3 of the height above the base. Chimney 25F-5 had two access doors at the base, and brick liner starting from the elevation 29.5 m till top of the chimney. Figure 3.1 shows the overall geometry of the chimney 25F-5 including large opening, access doors, and brick liner.

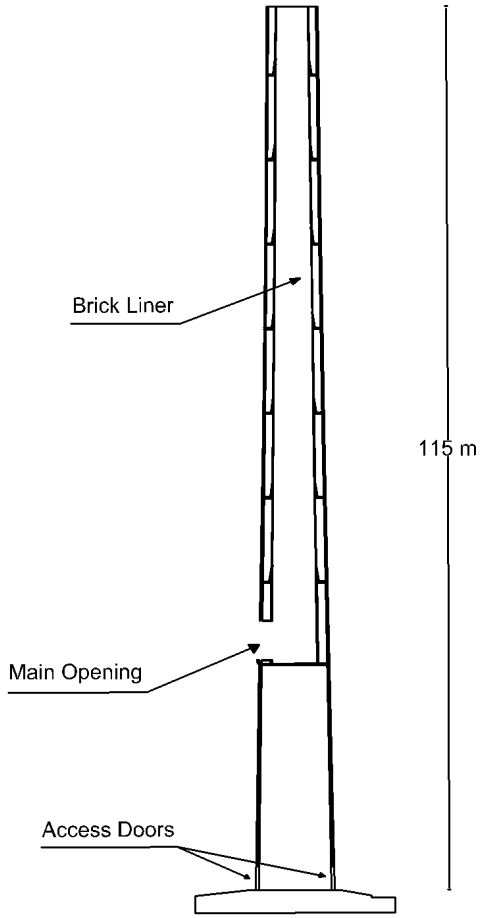

Figure 3.1. Vertical profile of the chimney 25F-5.

3.2. Chimney Openings

There were total of 3 openings located in the chimney 25F-5. Two minor openings as access doors existed at the base, and one major opening located at one third of the chimney height. Table 3.2 summarizes the diamaters, orientations and angles of the openings in chimney 25F-5. Figure 3.2 shows the plan view of the openings and their

locations with respect to horizontal coordinate system.

Table 3.2. Parameters of the openings in chimney 25F-5.

	Width (m)	**Height** (m)	**Angle** (deg)
Major opening	3.73	5.17	50
Access doors	2	3	24

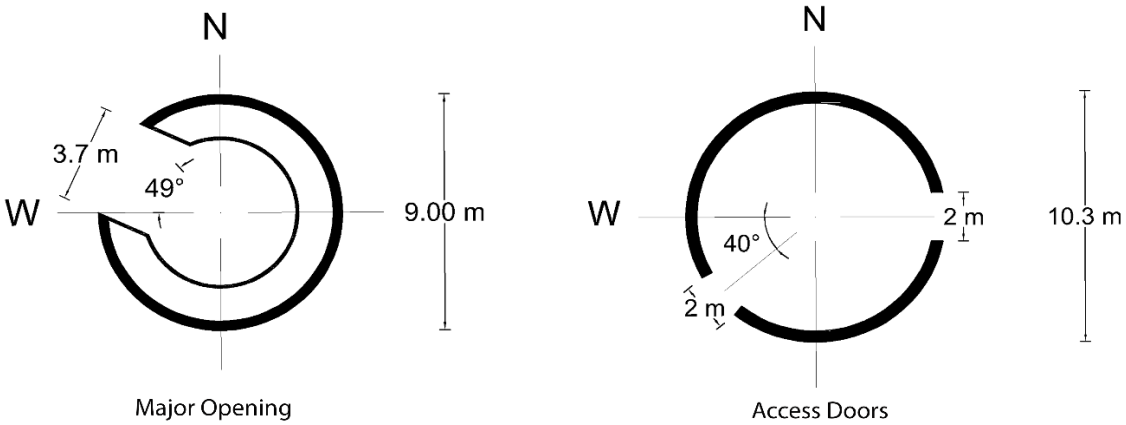

Figure 3.2. Opening details of the chimney 25F-5.

3.3. Chimney Windshield Reinforcement

RC chimneys are designed to resist the earthquake, wind and temperature loads. Vertical reinforcements are placed to provide flexural capacity at a cross section to resist moment demands coming from earthquake and wind excitations in RC chimneys. Moment demand distribution in RC chimneys decreases along the height. Therefore, vertical reinforcement ratio at the base is larger than the reinforcement ratio at the top. Vertical reinforcements are placed in a staggered pattern along the height of the RC chimneys. This results in discontinuity in vertical rebars, and proper lap slice distances needs to be provided to obtain the required flexural capacity at a cross section. Detailing of lap slice distances are provided in the ACI 307-69.

In chimney 25F-5, total length of the vertical rebars used changed from 6 m at the base to 4 m at the top of the chimney. Figure 3.3 shows the inner and outer vertical reinforcement distributions in chimney 25F-5 at the first 20 m for illustration purposes.

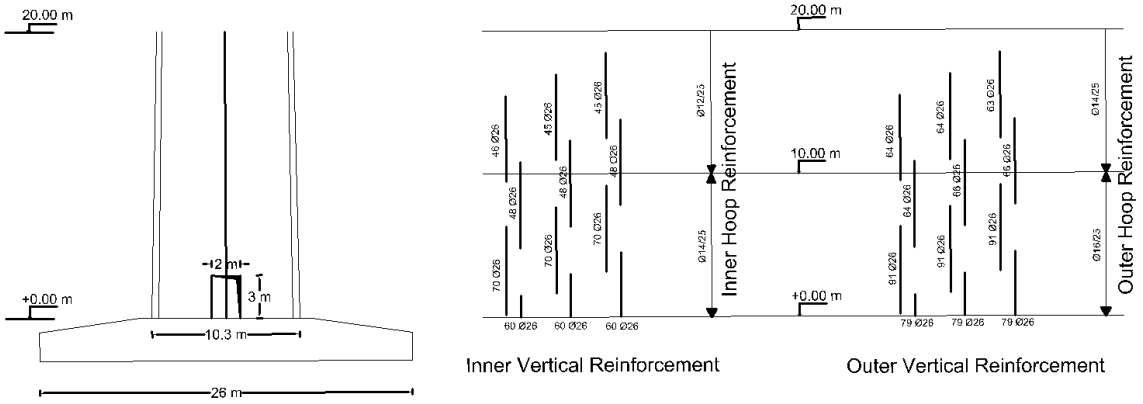

Figure 3.3. Inner and outer vertical reinforcement distributions of the chimney 25F-5.

Main purpose of RC chimneys is to dissipate toxic gases into atmosphere coming from the plant. Generally, temperature inside RC chimneys can reach up to 800 degree Celsius, which leads to expansion in the chimney cross section. In RC chimneys, hoop reinforcement is placed on the periphery of the cross section to resist the stresses coming from temperature loads. Tables 3.3 and 3.4 give the inner and outer hoop reinforcement distributions in chimney 25F-5, respectively.

Table 3.3. Inner hoop reinforcement distribution in chimney 25F-5.

Range (m)	**Amount** (bar/cm)
From 0 to 10	$\phi 14/25$
From 10 to 40	$\phi 12/25$
From 40 to 115	$\phi 10/25$

Table 3.4. Outer hoop reinforcement distribution in chimney 25F-5.

Range (m)	**Amount** (bar/cm)
From 0 to 10	$\phi 16/25$
From 10 to 40	$\phi 14/25$
From 40 to 115	$\phi 12/25$

3.4. Chimney Opening Reinforcement

RC chimneys are designed to withstand earthquake and wind loads which generate overturning moments over the height of the chimney. Concrete area is lost at a cross section where opening exists. Therefore, to provide enough flexural capacity in the opening region, additional vertical and horizontal reinforcements are placed at the sides and lintels of the opening, respectively. Apart from additional vertical and horizontal opening reinforcements, diagonal reinforcements are placed at the corners of the opening to prevent the crack formations under gravity and lateral service loads. Figure 3.4 shows the details of the additionl vertical, horizontal and diagonal opening reinforcements in chimney 25F-5.

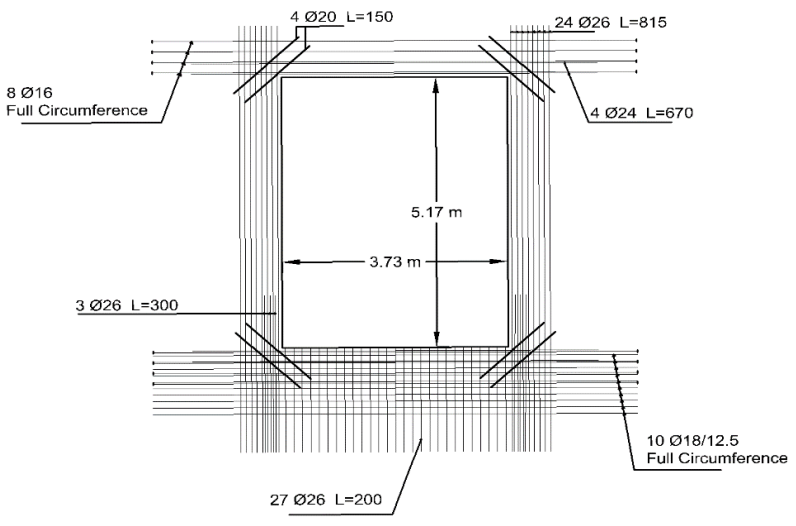

Figure 3.4. Opening reinforcement details of the chimney 25F-5.

3.5. Other Structural Components

One of the purposes of the chimney 25F5 was to discharge the flue gases coming from incinerators. Refractory bricks are used as a lining to prevent concrete windshield from hot flue gases. Brick liner contributed to almost 15% of the total weight of the chimney 25F-5. Therefore, it had major impact on the dynamic behavior of the chimney. In chimney 25F-5, brick liner was sitting on the corbel rings at each 11 m and the base of the brick liner was supported by the slab at an elevation of 29.5 m. Brick liner had a thickness of 20 cm up to elevation of 40 m. Above 40 m, thickness reduced to 10 cm and continued till the top of the chimney. Dimensions of the refractory brick was approximately 12x10x20 cm. Corbel rings were 20 cm thick reinforced concrete slabs, and they behaved in a cantilever manner hanging from chimney windshield. Therefore, they were not able to take any large vertical loads. Corbel rings were supported by inclined beams which carries the majority of the vertical loads. There is no any moment and shear transfer between brick liner and concrete windshield. Figure 3.5 shows the detail of the brick liner and corbel rings in chimney 25F-5.

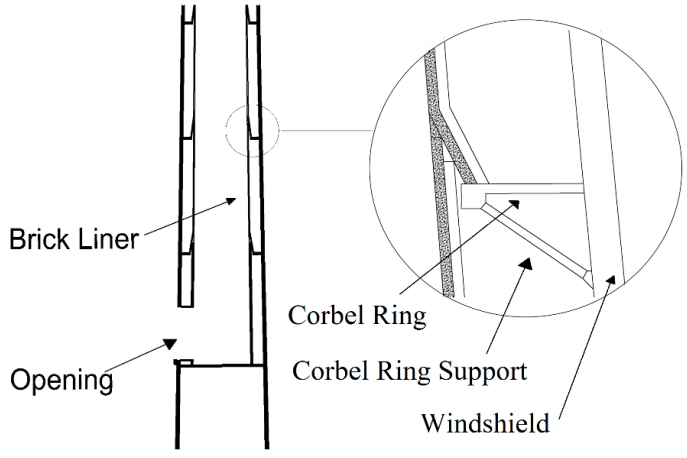

Figure 3.5. Brick liner and corbel ring details of the chimney 25F-5.

4. SELECTION OF THE NUMERICAL METHOD

In order to understand the effects of reinforcements on the behavior of RC chimneys under lateral and gravity service loads, crack developments at the opening region and stress concentrations in reinforcements and concrete windshield need to be investigated, which can only be achieved by explicitly taking into account all reinforcements. Simulations under lateral and gravity service loads were carried out using LS-Dyna [18] software package. Modeling chimney 25F-5 with 3D finite elements had some advantages and disadvantages in terms of investigating the effectiveness of the diagonal corner reinforcements.

(i) Advantages of using full 3D model.

- No geometric, constitutive and loading assumptions are required.
- Boundary conditions treated more realistically.
- Better visualization of the structure.

(i) Disadvantages of using 3D model.

- Requires higher effort in terms of mesh generation.
- Higher effort in terms of Post-Processing.
- Longer simulation run-time.

4.1. Solution Procedure

Nonlinear dynamic analysis of the chimney is conducted using LS-Dyna software package. LS-Dyna provides explicit time integration method in dynamic analysis. Explicit method is based on central difference algorithm [19–21]. The dynamic equilibrium of the explicit scheme is given in Equation 4.1. The right hand size of the equation consists of the external forces (f_n^{ext}) and the internal forces (f_n^{int}).

$$\left[M\right] \ddot{u}_n = f_n^{ext} - f_n^{int} \tag{4.1}$$

The Courant stability criterion limits the time step size to a smaller value in explicit method. Depending on the mesh size, time step in explicit method can be reduced to in the range of microseconds. Diagonal mass matrix $\left[M\right]$ used in the equation simplifies the solution significantly for the unknown acceleration vector $\ddot{u}_n$. The solution of the above equation is straightforward and does not require solution of linear system of equations.

4.2. Finite Element Formulations

Finite element and integration formulations were important in terms of accuracy and efficiency in the analyses. For each type of elements, several formulations exist based on the stress and strain distributions throughout the finite element.

Solid elements with 8-node, single integration point were used as hex elements in RC chimney windshield modeling. Since the stress was constant in the solid element, stress distribution was under integrated. However, it provided accurate and efficient results, and even works for severe deformations.

All reinforcing rebars were modeled with 2-node beam elements. Beam elements were sharing nodes with solid hex elements. Hughes-Liu with cross-section integration was used as beam finite element formulation.

4.3. Contact Mechanism

Contact mechanism in FE analyses allowed unmerged elements to interact with each other. There are many different contact algorithms currently implemented in LS-Dyna, each having various options and parameters. Penalty-based contact method was implemented in the analyses of the chimney 25F-5 under lateral and gravity service loads. Contact mechanism was defined for the brick liner, corbel rings and concrete windshield. Using contact algorithm, brick liner was modeled to sit on the corbel rings and no bending moments and shear forces were transfered to concrete windshield. This allowed to investigate the contribution of brick liner on the behavior of the chimney 25F-5.

4.4. Concrete Material Model

LS-Dyna software offers a wide range of non-linear material models for simulating the behavior of concrete. These models differ from each other in terms of defined failure or yield criterion, consideration of the tri–axial state of stress, cyclic behavior under tension and compression, compression strain softening, post–cracking response such as shear transfer after cracking or tension stiffening [22]. The Winfrith concrete model was selected to characterize the behavior of concrete windshield [23, 24].

4.4.1. Ottosen Failure Surface

The Winfrith concrete model utilizes Ottosen failure surface [25] as a limiting ultimate strength for the concrete given in Equation (4.2). The failure surface shape is defined by the constants A and B, and by the parameter λ, which is a function of the principal stresses σ_1, σ_2, and σ_3. The first invariant of the stress tensor I_1 and the second invariant of the deviatoric stresses J_2 are given in Equations (4.3) and (4.4), respectively.

The concrete compressive strength is represented by f_c. The A and B constants are computed internally in the LS-Dyna solver from the user-specified concrete compressive strength f_c.

$$A\frac{J_2}{(f_c)^2} + \lambda\frac{\sqrt{J_2}}{f_c} + B\frac{I_1}{f_c} = 1 \tag{4.2}$$

$$I_1 = \sigma_1 + \sigma_2 + \sigma_3 \tag{4.3}$$

$$J_2 = \frac{1}{6}\{(\sigma_1 - \sigma_2)^2 + (\sigma_2 - \sigma_3)^2 + (\sigma_3 - \sigma_1)^2\} \tag{4.4}$$

The Winfrith concrete model is chosen for the analysis of the chimney due to its ability to represent the triaxial failure state of concrete.

4.4.2. Concrete Model under Tension

Concrete model under tension is assumed to follow a tri-linear relationship. The slope of the increasing part (prior to cracking) is equal to the elastic modulus of the concrete. The decreasing part (after cracking) is a stress function which is dependent on the crack width. After the cracking of concrete, the crack normal stress reduces following a bilinear decay function, which is an approximation of the tension–softening property of the concrete. Figure 4.1 shows the cyclic behavior of concrete under tensile loading. Plain concrete physically displays strength degradation during unloading after cracking. However the Winfrith concrete model forms a linear elastic path during unloading and reloading. Failure of concrete in tension is achieved after tracing the decay function when the strain in the finite element reaches to the ultimate strain value.

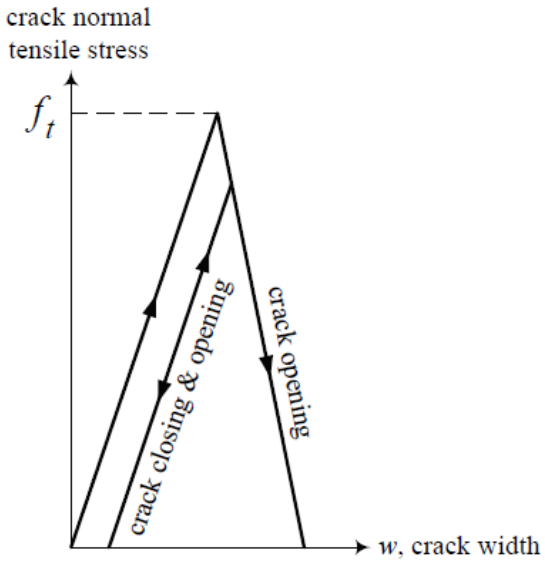

Figure 4.1. Crack width and behavior of Winfrith concrete under tension.

4.4.3. Concrete Model under Compression

The stress-strain relationship of the concrete model has a very simple shape which is formed with a bilinear curve under compressive loading. The ultimate compressive strength, f_c, is limited with the Ottosen failure surface that takes into account the tri-axial state of stress. The effect of confinement is incorporated in the Winfrith concrete model. An increase in compressive stresses in the direction of two orthogonal axes results in an increase on the compressive strength in the third direction. On the contrary to the effect of confinement, suction stresses in the direction of two orthogonal axes causes a reduction on the compressive strength in the direction of the third axis perpendicular to the other two orthogonal axes. Concrete in compression during unloading and reloading is assumed to behave linearly elastic with a slope equal to the elastic modulus of concrete. Figure 4.2 shows the stress-strain relationship of concrete in compression under cyclic loading. Failure under compression is achieved when the strain value in the finite element reaches an ultimate compressive strain.

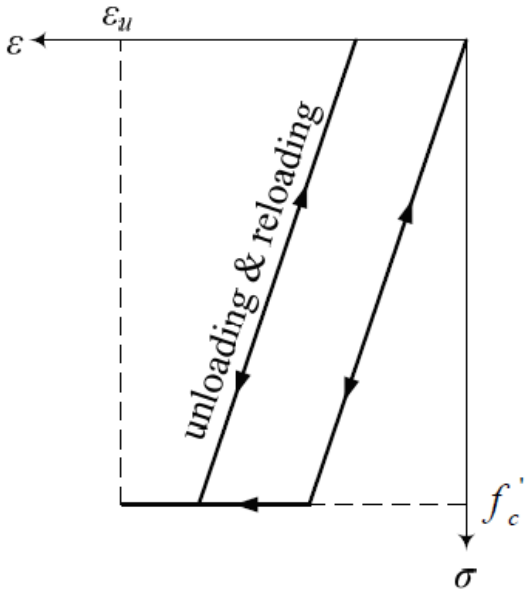

Figure 4.2. Behavior of Winfrith concrete under compression.

4.4.4. Concrete Model under Shear

The Winfrith concrete model takes into account the shear force transfer due to aggregate interlock parallel to the cracked section. Shear stress at the finite element is multiplied by a coefficient which is dependent on the crack width and consequently on the aggregate diameter to reduce the transferred shear stress. Shear stress modification coefficient, SSC, versus crack width relationship is given in Equation 4.5.

$$SSC = \frac{(a-w)^2}{a^2} \tag{4.5}$$

In the equation above, a is the aggregate diameter defined by the user and w is the crack width at the current time step. Figure 4.3 demonstrates the relationship of shear stress transfer in concrete model. It should be noted that when the crack width exceeds the aggregate diameter no shear stress is transferred. On the other hand, if the crack is closed, the shear stress is transferred without any reduction.

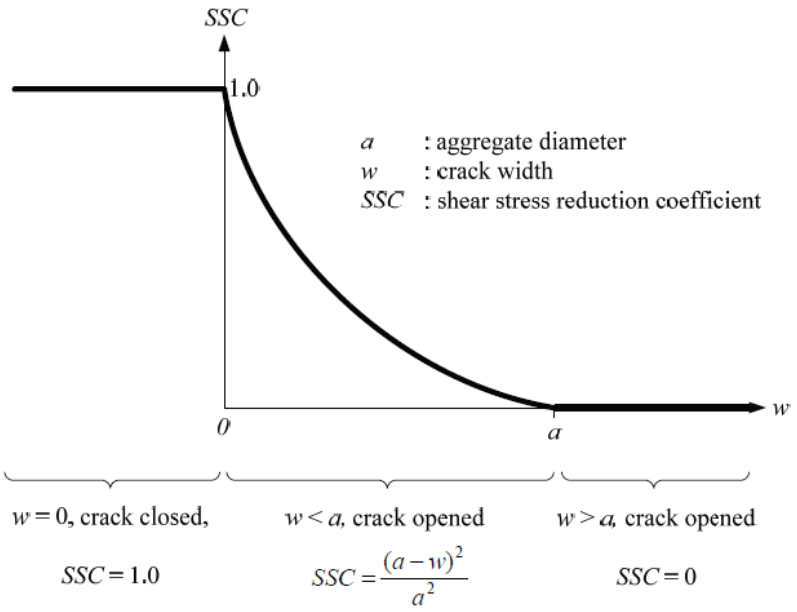

Figure 4.3. Behavior of Winfrith concrete under shear.

The concrete classification of the 25F-5 chimney was "B-300 grade" with a compressive cylindrical strength f_c of 25 MPa. The tensile strength was assumed to be 10% of f_c. The concrete elastic modulus and Poisson's ratio were assumed as 30 GPa and 0.2, respectively. The concrete density, crack width, and shear-interlocking aggregate size were assumed as 2400 kg/m^3, 5.08E-6 m and 0.019 m, respectively.

Material parameters were calibrated by using the experimental results of John L. Wilson's previous CICIND-sponsored research project back in 2003. The results of the calibration study was presented by Sami A. Kilic at the 2014 CICIND Prague Meeting. Results of finite element analysis captured the failure envelope of the test results but showed a stiffer response in general. The crack formation in the finite element results showed agreement with the cracks observed in the experimental study [26, 27].

Moreover, Selcuk Altay used the Winfrith concrete model on the cyclic hysteretic response of T-shaped beam-column exterior joint assemblies on his Ph.D. thesis in 2010 [28]. The Winfrith concrete material model provided good agreement with the experimental results.

4.5. Reinforcement Material Model

The Plastic-Kinematic material model of the LS-Dyna code was used for the rebars. Stress-strain constitutive relationship of the reinforcement is simulated with a bilinear curve, whose initial slope is equal to the Young's Modulus of the steel. Elastic behavior of the steel reinforcing material is limited by the yield stress provided by the user as an input. The second portion of the bilinear curve is assumed to simulate the behavior of the reinforcing steel after yielding occurred. After yielding, plastic deformations are allowed and the slope of the unloading-reloading stress-strain curve is kept equal to the Young's Modulus of the steel material. Under cyclic loading, the model displays an isotropic hardening rule. This enables the yield surface to expand under plastic cyclic deformations. Figure 4.4 shows the stress-strain relationship of reinforcing steel material under cyclic loading. In the analyses, yield strength f_y, ultimate strength f_u, and elastic modulus were assumed as 420 MPa, 550 MPa, and 200 GPa, respectively. The Poisson's ratio was 0.3 and the steel density was 7800 kg/m^3.

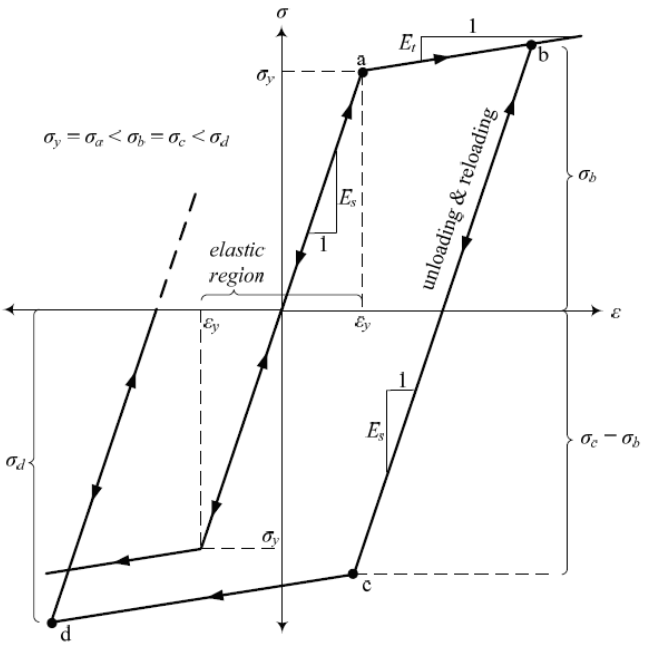

Figure 4.4. Stress-strain relationship for reinforcement material model.

4.6. Brick Liner and Corbel Ring Material Models

The brick liner was modeled with an elastic material model in the current study. Future work will involve the development of a brittle material model with failure (disintegration) capabilities. Density of the refractory brick was assumed as 2100 kg/m^3. Elastic modulus and Poisson's ratio were 20 GPa and 0.2, respectively.

Rigid material model of the LS-Dyna code was used for the corbel rings. Density, elastic modulus, and Poisson's ratio were assumed as 2500 kg/m^3, 30 GPa, and 0.2, respectively.

The inclined support beams were modeled with elastic material properties. Due to the lack of material data for the support beams, elastic steel material properties were used. Elastic modulus and Poisson's ratio were assumed as 200 GPa and 0.3, respectively.

5. FE MODELING OF THE RC CHIMNEY

Typical mesh generation process involves the use of a graphical user interface by point-and-click type of operations. Parametric mesh generation allows flexibility in terms of altering and generating the finite element model of the structure. Full 3D model of the chimney 25F-5 was created using the parametric finite element meshing software package TrueGrid [29]. Material and geometric properties were obtained from the drawings provided by Endem Construction Ltd. Vertical and horizontal reinforcement locations, opening reinforcement details, shell thicknesses, opening heights, and opening dimensions were the main characteristics of the chimney 25F-5. Chimney structure had a conical tapered shape with varying outer and inner slopes at different elevations. This required a special consideration in the mesh generation process. However, TrueGrid allowed the modeling of the chimney 25F-5 with few lines of programming codes. Moreover, parametric equations, arrays, control statements of the TrueGrid package allowed the user to model the structure more efficiently. Mesh refinement and alteration were easily carried out once the model was generated [30].

5.1. Mesh Resolution of the FE Model

In the initial modeling of the chimney 25F-5, entire vertical, hoop, and opening rebars were individually and explicitly modeled by beam finite elements. Resulting mesh size of the FE model reached approximately 7 million elements. High-resolution model of the chimney 25F-5 was called Model 1.

The computer run-time of the high-resolution Model 1 took in excess of 7 days on a parallel computing cluster of 4 servers, 32 processors, and 256 GB of RAM memory. Therefore, mesh coarsening and a reduction in the mesh resolution were inevitable. The parametric modeling capabilities of the Truegrid code were utilized in order to decrease the mesh resolution without regenerating the entire finite element mesh. The resulting mesh was regarded as the medium-resolution Model 2. The transition from the high-resolution to the medium-resolution model was made without altering the

reinforcement ratio and staggered pattern of the vertical reinforcement (lap splices). The number of rebars was reduced to four times by lumping the cross-sectional area of four rebars into one large rebar. Therefore, a significant saving was obtained in the total number of elements that were generated. The staggered pattern of the vertical reinforcement significantly influenced the vertical mesh generation process.

Dimensions of the hexahedral and beam finite elements were not smilar for Models 1 and 2. Figure 5.1 shows the relative comparison of the finite elements for Models 1 and 2 and the node sharing between hexahedral concrete and beam rebar finite elements. Hexahedral finite element dimensions were 10.9x4.6x4.9 cm for Model 1 and 10.9x18.4x19.9 cm for Model 2.

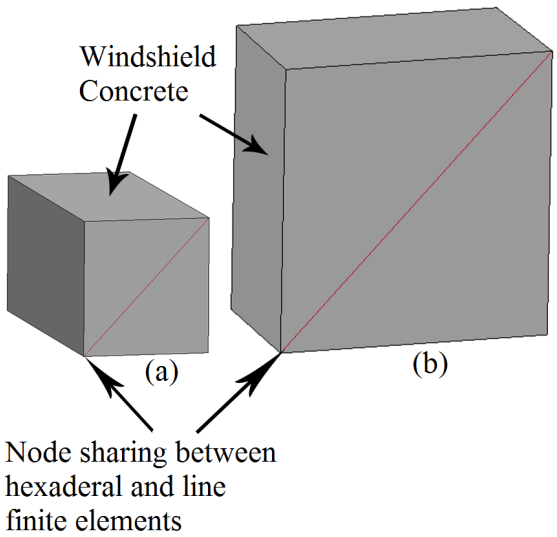

Figure 5.1. Mesh resolution and node sharing of finite elements; (a) Model 1, (b) Model 2.

Number of vertical reinforcements at a cross section along the height of the chimney was reduced four times for Model 2. Cross section labeled as "A-A" as shown in Figure 5.2 was cut at an elevation of 10 m to calculate and compare the flexural capacities of the Models 1 and 2. The cross section "A-A" had an outer diameter of 9.7 m and a wall thickness of 0.39 m. In Model 1, there were a total of 135 ϕ26 inner vertical and 191 ϕ26 outer vertical reinforcements. Model 2 had a total of 34

ϕ52 inner vertical and 48 ϕ52 outer vertical reinforcements. The reason for using the rebar size of ϕ52 was caused by the fact that four ϕ26 rebars were lumped into a single large rebar. Therefore, the cross-sectional area of ϕ52 corresponded to the sum of the cross-sectional areas of four ϕ26 rebars.

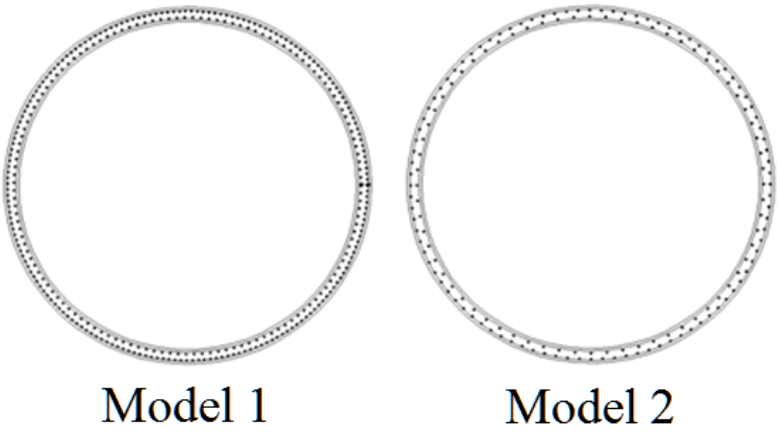

Figure 5.2. Layout of vertical reinforcements of the cross section "A-A" for the high-resolution Model 1 and medium-resolution Model 2.

Flexural strengths in the absence of an axial load for Models 1 and 2 were calculated using an external reinforced concrete section capacity analysis tool. The moment capacities for Models 1 and 2 were 321 and 323 $MN - m$, respectively. Flexural capacities were in good agreement for Models 1 and 2. Therefore, Model 2 was used in the simulations due to reduced number of elemenets and computational run-time.

5.2. FE Model of the Chimney 25F-5

Windshield concrete of the chimney was modeled using 8-node volumetric hexahedral finite elements, which corresponds to forming tapered cylindrical shape of the chimney 25F-5. Three main axes were radial, angular and vertical. In the radial direction, four hexahedral elements were generated through the thickness of the windshield. Outer and inner elements had 5 cm length in the radial direction, standing for 5 cm concrete cover used in the construction of the chimney. Middle elements separated outer and inner reinforcing rebars located in the chimney windshield. Angular meshes were

generated at every 2.4 degrees. This allowed the model to incorporate 150 different nodal locations in the periphery of the chimney concrete windshield in order to insert the vertical reinforcements. Vertical reinforcing rebars were uniformly distributed inside the windshield, and their total number was decreasing along the height of the chimney. Therefore, vertical reinforcements were inserted at different nodal locations in the mesh.

The uniform distribution of vertical rebars around the periphery of the chimney allowed a close representation of the actual chimney structure. The typical edge length of the hexahedral elements in the vertical direction was 20 *cm*. Vertical rebars were placed in a staggering pattern along the height of the chimney. Therefore, mesh nodes were created at the exact beginning and ending points of the vertical rebars, which made it possible to place the vertical rebars at the correct elevations along the chimney windshield. Figure 5.3 shows the FE models of the vertical profile, brick liner, corbel ring and corbel ring support in chimney 25F-5.

Total number of finite elements used in the chimney 25F-5 medium-resolution Model 2 was equal to 675065. Number of solid and beam elements were 451279 and 223786, respectively. 669065 of the elements were deformable and 6000 of them were rigid elements.

Outer and inner surfaces of the chimney adapted to a conical shape. Separate conical surfaces were generated for the inner and outer surfaces of the chimney concrete windshield. The specified concrete cover was 5 *cm*. Therefore, two additional conical surfaces were generated inside the thickness region of the chimney windshield that lied outside the concrete cover zones. Wall thickness of the chimney windshield increased from top to bottom. Therefore, thickness of the middle shell section also increased from top to bottom of the chimney structure. Another conical surface was formed corresponding to mid-point of the windshield thickness. A total of 5 conical surfaces were formed and the original cylindrical surfaces were projected to the corresponding conical surfaces.

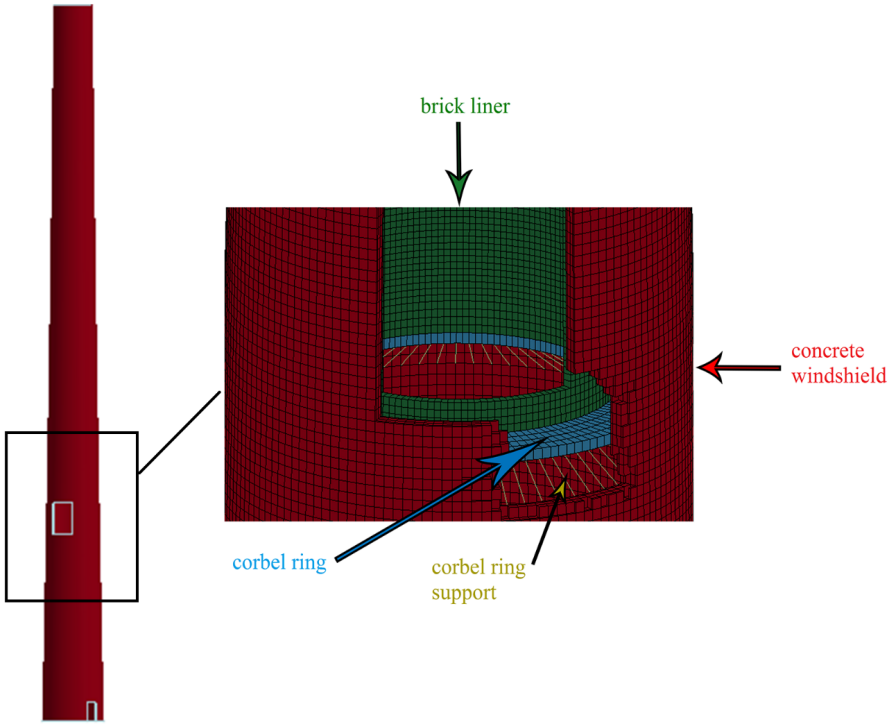

Figure 5.3. FE model of the chimney 25F-5.

There were a total of 3 openings located in the 25F-5 chimney. Two minor openings of access doors existed at the base, and one major opening was located at one third of the height. The locations and dimensions of the three openings were given in the design documents. The hexahedral finite elements in the opening regions were deleted from the mesh.

The finite element modeling efforts using the TrueGrid software can actually yield a mesh that takes into account the discontinuity of the vertical reinforcement with the staggered layout. Vertical and horizontal reinforcements were generated with simple line of codes. The only necessary information required was their locations. After obtaining the vertical and horizontal reinforcement locations from the design drawings, the beam finite elements representing the rebars was generated in the model at the exact locations.

Figure 5.4 illustrates the staggered vertical and hoop reinforcement details in the finite element model. The layers of vertical rebars were not placed along the same vertical line in order to model the discontinuity and the overlapping effect. The concrete hexahedral elements shared nodes with the line finite elements representing the reinforcements.

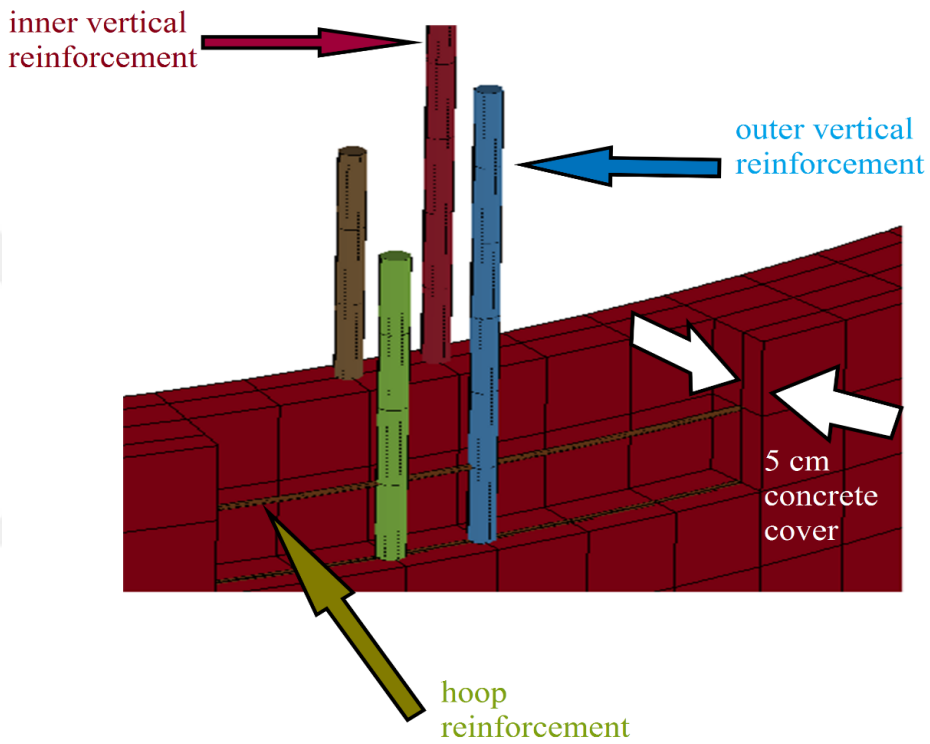

Figure 5.4. FE model of the vertical and hoop reinforcements.

Additional vertical and horizontal opening reinforcements were generated in a same manner as above. Locations of the additional opening reinforcements were obtained from structural drawings of the chimney 25F-5. Using beam finite elements, opening reinforcement rebars were generated in the model at the exact locations.

Brick liner and corbel rings were modeled explicitly in the FE model. Refractory bricks and corbel rings were modeled also using solid hex elements. Corbel rings were attached to chimney windshield by means of sharing nodes with each other. Brick liner was sitting on top of corbel ribgs and they did not share any nodes. Contact mechanism

was constructed between corbel rings and brick liner, which will transform loads from brick liner to corbel rings when they are in contact. Inclined corbel ring supports were modeled using line finite elements. They share nodes with corbel rings and concrete windshield at the same time. Figure 5.5 shows the explicit modeling of the concrete windshield, brick liner, corbel ring and corbel ring supports of the regenerated model.

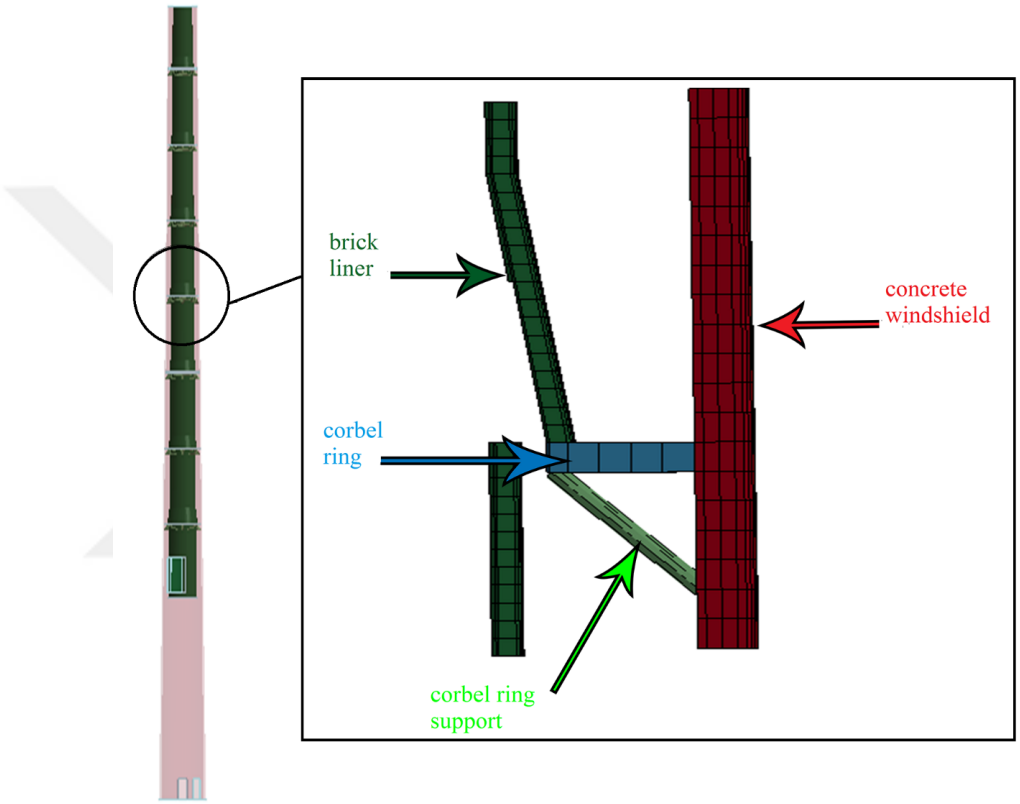

Figure 5.5. FE model of the brick liner and corbel rings.

5.3. FE Model of the Diagonal Corner Reinforcement

The projection of the diagonal corner rebar onto the vertical plane was 45 degrees. Due to the curved geometry of the circular concrete windshield, the beam finite elements of the diagonal rebar had to be inserted along a curvilinear or skewed path. In order to properly model the coupling between the diagonal rebar and the surrounding hexahedral concrete elements, the beam finite elements of the rebar had to share nodes with the hexahedral elements. The inclination of the diagonal beam elements

was approximately 45 degrees. Figure 5.6 illustrates the diagonal opening corner reinforcements detailing of the finite element model.

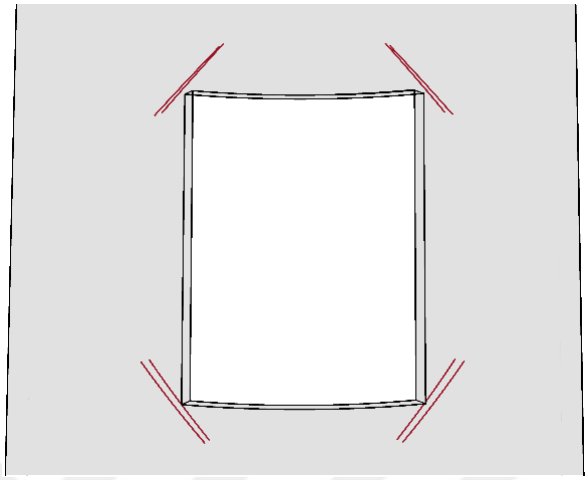

Figure 5.6. FE model of the diagonal opening corner reinforcements.

5.4. FE Model of the Vertical and Horizontal Corner Reinforcement

Aim of the thesis study was to investigate whether vertical and horizontal opening corner reinforcements can be as effective as diagonal opening reinforcements in RC chimneys in terms of preventing crack formations at the corners of the opening. Figure 5.7 shows the design alternative of using single vertical and horizontal reinforcements that replaced each diagonal rebar at the four corners. The vertical and horizontal reinforcements had the same diameter as the diagonal rebars. The original design had 4 diagonal rebars at each corner that resulted in a total number of 16 rebars for the entire opening. The alternative design approach yielded 4 vertical and 4 horizontal rebars at each corner that required the use of 32 rebars for the opening region. The length of the diagonal, horizontal, and vertical rebars were equal to 1.5 m.

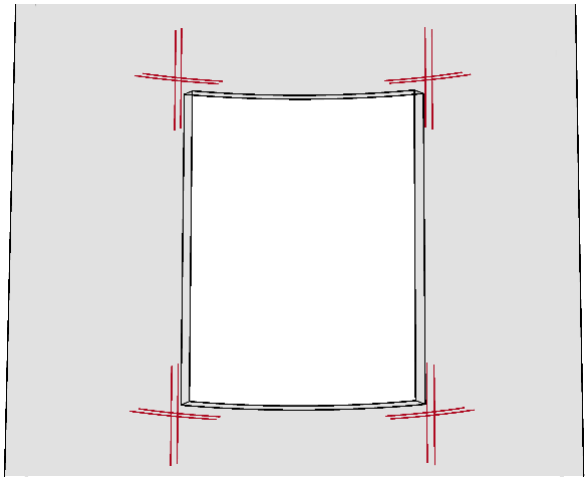

Figure 5.7. FE model of the vertical and horizontal opening corner reinforcements.

5.5. Boundary Conditions of the Chimney 25F-5

Chimney 25F-5 had 284 foundation piles at the site. Base of the chimney was assumed to be fixed, with no SSI condition. Base of the chimney was fixed in translation and rotation in the global X, Y, and Z directions in the FE model. Figure 5.8 shows the boundary condition of the chimney 25F-5 under gravity and lateral service loads.

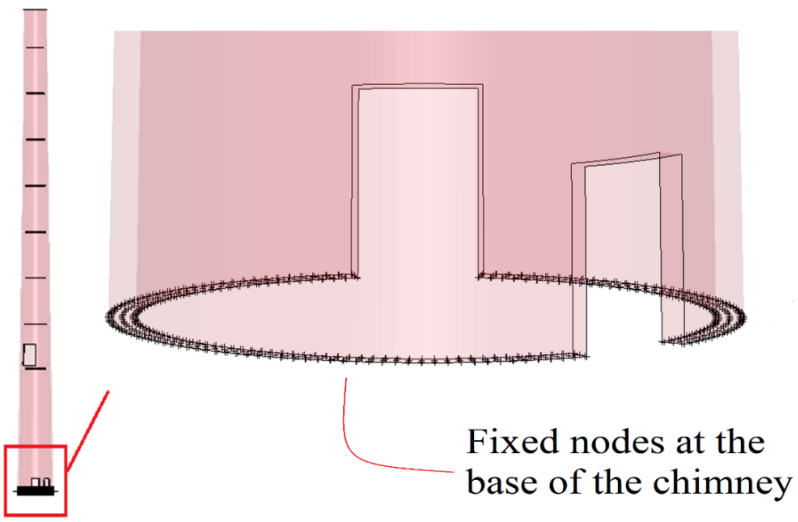

Figure 5.8. FE model of the boundary conditions in chimney 25F-5.

5.6. Loading Conditions of the Chimney 25F-5

The response of the chimney 25F-5 was investigated under lateral and gravity service loads. First, gravity loads were applied within 1 seconds as a body load on the structure. Dynamic effects were eliminated by assigning global damping value. Afterwards, lateral pressure loads were applied within 2.5 seconds on the chimney 25F-5 in the opposite direction of the opening. The magnitude and pattern of the lateral pressure loads were in accordance with the design wind load calculations of the chimney 25F-5, which were obtained from the original design documents. Figure 5.9 shows the magnitude and distribution of the applied lateral pressure loads on the chimney 25F-5.

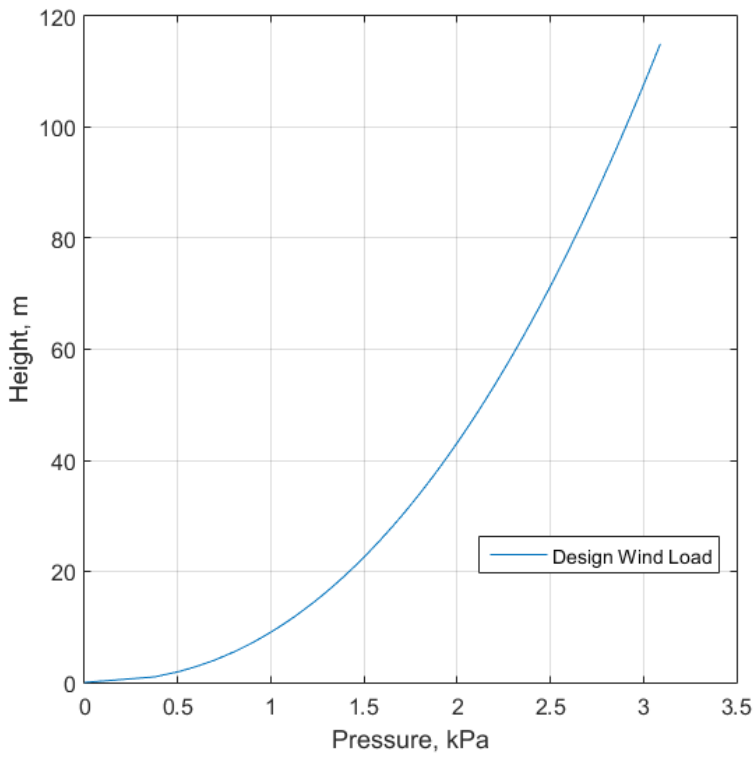

Figure 5.9. Lateral service loads.

6. SIMULATION RESULTS UNDER GRAVITY SERVICE LOADS

Chimney 25F-5 was analyzed under gravity service loads for the original design method using diagonal opening reinforcements and alternative design method suggesting vertical and horizontal opening corner reinforcements. Response of the chimney under gravity service loads was investigated and the results were compared for two different design methods in terms of stress and strain distributions around the opening and at the corner reinforcements.

6.1. Validation of the FE Model

Full 3D FE model was used to carry out the simulations under gravity and lateral service loads. Validation and comparison of the Models 1 and 2 were porformed by examinig the total energies, weights and vertical displacements under gravity service loads. Table 6.1 gives the simulation run-times for Models 1 and 2 under gravity service loads applied in 1 seconds for the original design method. The numerical analyses were done by using a parallel computing cluster system with 4 servers, 32 processors, and 256 GB of RAM memory. The run-times for Model 1 prohibited its practical use for parametric studies. Therefore, further simulations of the thesis study utilized Model 2.

Table 6.1. Simulation run-times for Models 1 and 2.

Simulation	**Computer Run-time (hours)**	**Computer Run-time (days)**
Model 1	192	8
Model 2	12	0.5

Figures 6.1 and 6.2 illustrate the total, kinetic, internal (strain energy), hourglass, and damping energies for Models 1 and 2. In the simulations, loading was applied dynamically within 1 seconds. The steady state solution was obtained after the 0.8 *sec* time mark in each simulation. The FE analyses could be incorporated as quasi-static, since the kinetic energy during the analyses was close to zero and the internal strain energy, which occurred as a result of the chimney deformations, was in close agreement with the total energy of the finite element simulations. Negligible amounts of energy were dissipated in terms of the hourglass and damping components. The total energies of both simulations were in the order of 25 KJ.

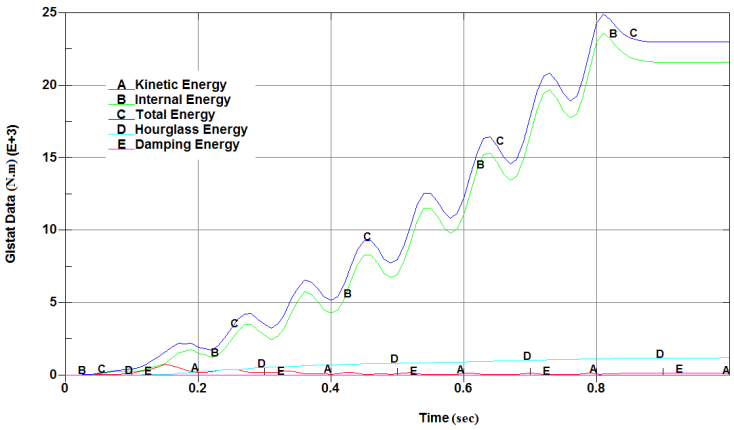

Figure 6.1. Evolution of energies for Model 1 under gravity service loads.

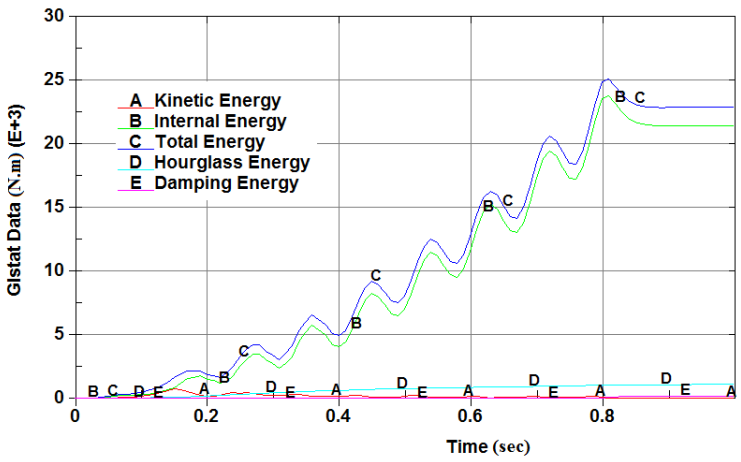

Figure 6.2. Evolution of energies for Model 2 under gravity service loads.

The axial load at the base and top displacement of the chimney 25F-5 under gravity service loads were calculated by using an analytical approach. The results of the finite element analyses were compared with the analytical calculations for the orginal design method. This approach enabled the validation of the numerical results of the FE analyses. The structural components of the chimney, such as the brick liner or opening reinforcements, can be included or excluded in the finite element simulations.

Structural components of the chimney 25F-5 were concrete windshield, corbel rings, and brick liner. The total weight of the chimney was calculated by adding the individual weights of various structural components. Table 6.2 provides the calculated weights of the structural components of chimney 25F-5.

Table 6.2. Weights of the structural components of the chimney 25F-5.

Structural Component	**Weight** (kN)
Windshield	21524
Brick Liner	3173
Corbel Ring	1124

Total weight of the entire chimney was obtained by summing the weights of the structural components, which was equal to 25821 kN. Total axial load at the base of the chimney obtained from LS-Dyna analyses of the high-resolution Model 1 and medium-resolution Model 2 are illustrated in Figures 6.3 and 6.4. The body loading of the gravity simulations were applied dynamically as a ramp function. The body loads were applied in 0.8 *sec*, and kept constant until the final simulation time of 1.0 *sec*. The vibrations that occurred in the initial 0.8 *sec* were damped out by viscous damping. The high frequency oscillations between 0.2 and 0.4 *sec* were caused by the contact between the brick liner and corbel rings. The oscillations ceased after 0.4 *sec* when the contact equilibrium was reached. The steady state solution was reached at the end of 1.0 *sec* in both simulations. The analytical calculations also confirmed the validity of the steady state solutions of the LS-Dyna simulations.

The total weight of the chimney for Models 1 and 2 were obtained as 24980 and 24940 kN, respectively. Therefore, the total chimney weight of Model 2 was in close agreement with both the Model 1 and analytical calculations.

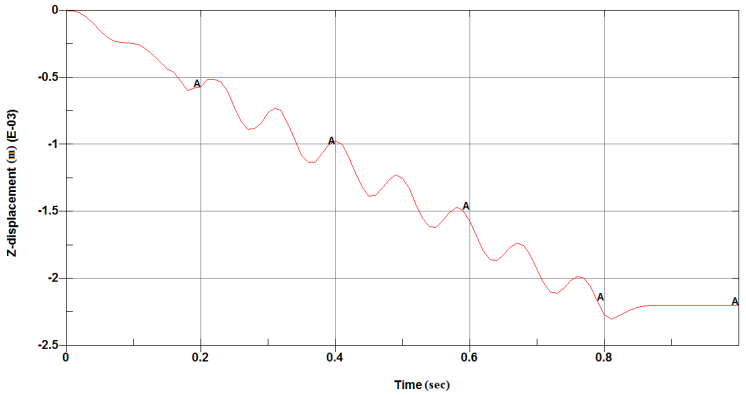

Figure 6.3. Total weight of the chimney 25F-5 for Model 1.

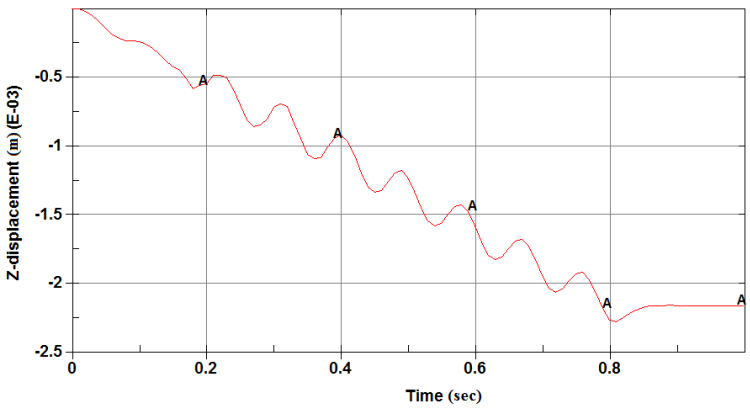

Figure 6.4. Total weight of the chimney 25F-5 for Model 2.

The top displacement of the chimney 25F-5 was calculated by considering the continuous masses of the concrete windshield, corbel rings and brick liner under gravity service loads. The vertical reinforcement ratio was 1.59% and 0.29% at the bottom and top of the chimney, respectively. The effect of the vertical reinforcements on the top displacement was negligible because RC chimneys are very rigid structures in the longitudinal profile. Therefore, the vertical reinforcements were not taken into account in the analytical calculations. The chimney 25F-5 consisted of multiple tapered segments along the height.

The weights of the brick liner and corbel rings were considered as continuous masses that were smeared along the height of the chimney. The total weight of the chimney used in the displacement calculation was taken as 24980 kN. Top vertical displacement of the chimney 25F-5 under gravity service loads was calculated as 1.9 mm. The time history of the top vertical displacement for Model 1 is shown in Figure 6.5. The steady state solution was reached at a top vertical displacement value of 2.20 mm. The time history of the top vertical displacement for Model 2 is shown in Figure 6.6. The steady state solution was reached at a top vertical displacement value of 2.16 mm. The top vertical displacement of Model 2 was in close agreement with both the Model 1 and analytical calculation results.

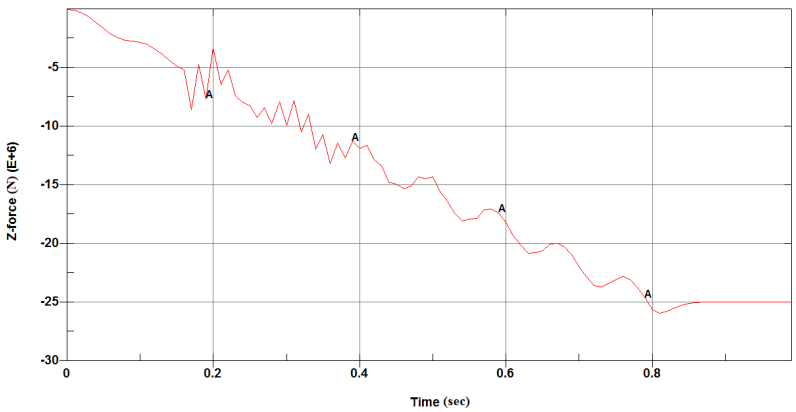

Figure 6.5. Top vertical displacement time history for Model 1.

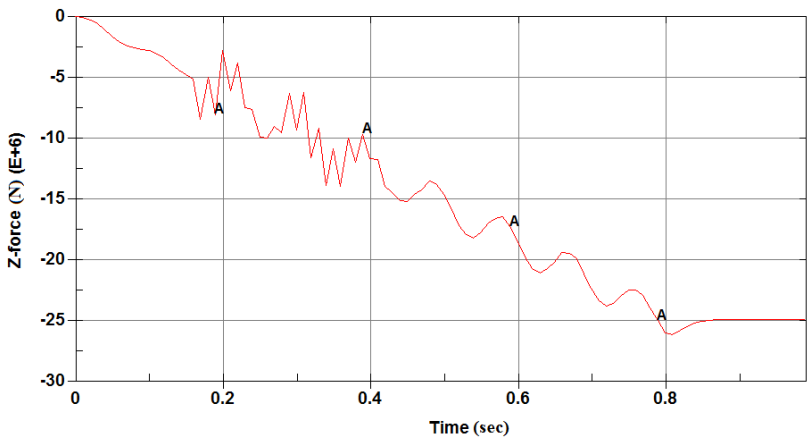

Figure 6.6. Top vertical displacement time history for Model 2.

An eigenvalue analysis was conducted to compute the mode shapes and frequencies of the chimney 25F-5. Table 6.3 shows the first four mode periods of the chimney. First mode of the structure was in the direction of the opening with period of 1.65 *sec*. Second mode of the structure was in the orthogonal direction of the opening with period of 1.61 *sec*. The ACI 307-08 code provides a formula for the calculation of the first mode period to be used in the preliminary design of chimneys. The computed period is also presented in Table 6.3.

Table 6.3. Modal periods of the chimney 25F-5.

Mode	**FE Analysis Period** (*sec*)	**ACI 307 Period** (*sec*)
1	1.65	1.49
2	1.61	
3	0.38	
4	0.37	

Figure 6.7 shows the mode shapes of the first two modes of the chimney. Chimney 25F-5 has two natural modes of vibrations which were in the opening and orthogonal to the opening directions.

The finite element eigenvalue analysis yielded different modal periods in the direction of the opening when compared to the orthogonal direction. The existence of the opening influenced the modal periods in different directions of vibration as expected. However, the ACI 307 Code preliminary design formula for calculating the period of the first fundamental mode assumes a fully continuous windshield with no opening discontinuity, which causes the calculated period to be shorter than the finite element computation.

Analyses results of Model 1 and 2 were in good agreement. Moreover, results obtained from simulations were acceptable, since they were close to the calculated analytical results. Model 2 will be used for further analyses in comparing the results of the design configurations under gravity and lateral service loads.

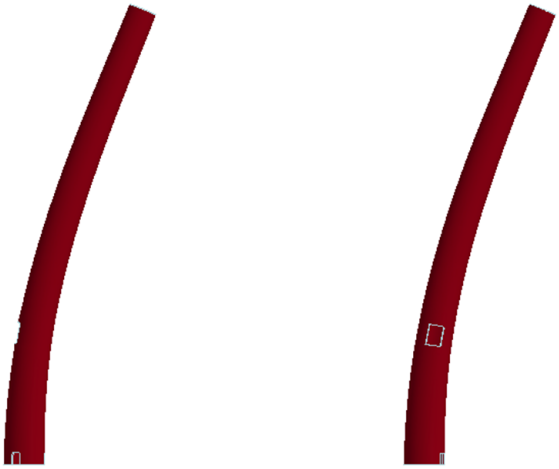

Figure 6.7. Mode shapes of 25F-5, (a) 1st mode, T1 = 1.65 *sec*, (b) 2nd mode, T2 = 1.61 *sec*.

6.2. Comparison of Design Alternatives under Gravity Service Loads

Chimney 25F-5 was analyzed for the original design with diagonal corner rebars (Case 1) and the alternative design solution with horizontal and vertical corner rebars (Case 2) under gravity service loads. This section provides comparisons of the two different corner reinforcement configurations in terms of the stress concentrations around the opening and stresses at the corner reinforcements.

Stresses were concentrated at the opening region under gravity service loads for both design cases. Main reason was that opening regions are weak zones in RC chimneys due to the missing of concrete area. The upper and lower lintels were unsupported vertically along their spans as a result of the opening, similar to deep RC beams with fixed ends. Tensile stresses were developed at the lintes under gravity service loads. Stress plots around the opening were investigated in detail in order to understand the concentration of stresses in critical regions. Figures 6.8 and 6.9 show the contours of minimum principal stress distributions at the opening region for Case 1 and 2 under gravity service loads, respectively.

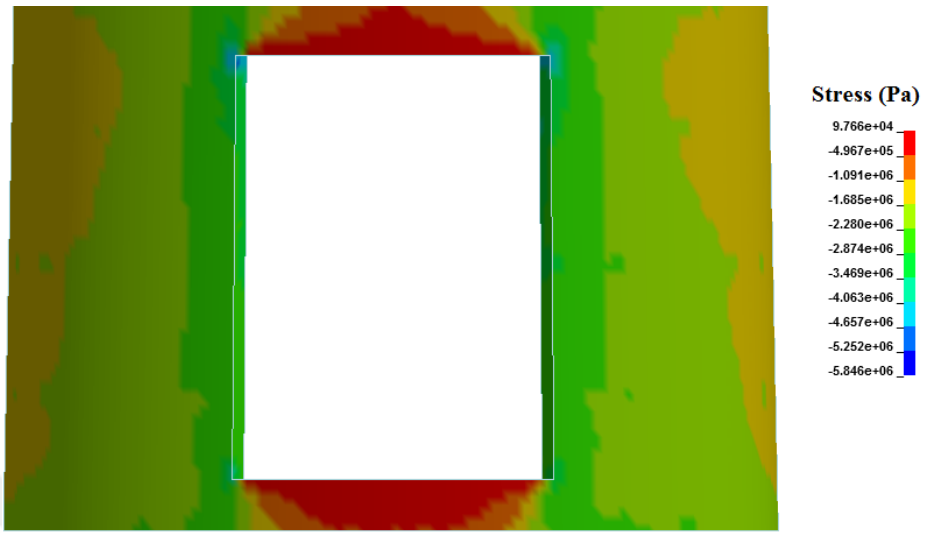

Figure 6.8. Contours of minimum principal stresses for Case 1 under gravity service loads.

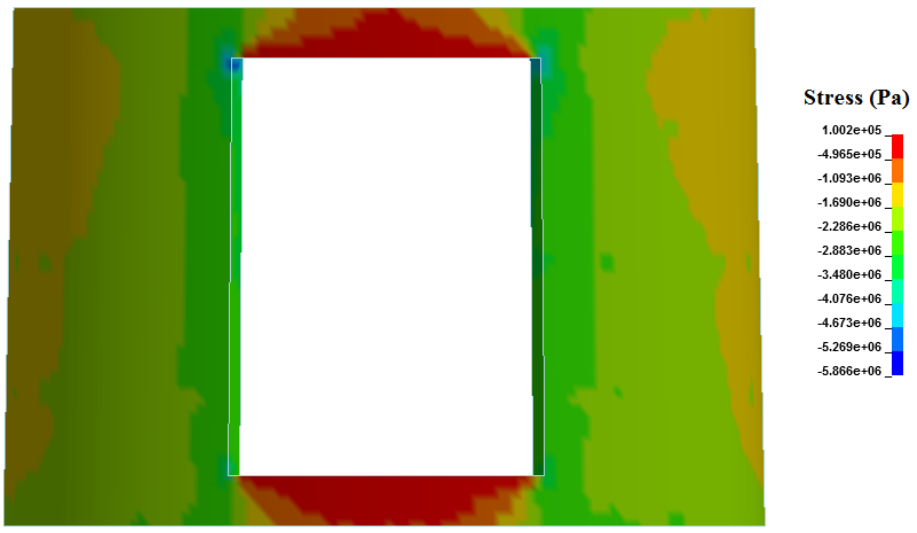

Figure 6.9. Contours of minimum principal stresses for Case 2 under gravity service loads.

Maximum tensile stresses occurred at the inner surface of the top lintel for both cases, which were equal to 2.1 MPa. Maximum compressive stresses occurred at the top left corner of the opening for both Case 1 and 2, which were equal to 5.85 and 5.87 MPa, respectively. Crack formations were not observed under gravity service loads. Distributions of the maximum and minimum principal stresses around the opening region were not uniform. Tensile stresses developed at the top and bottom lintels. However, compressive stresses developed at the side walls and corners of the opening. The stress distributions through the thickness of the concrete wall in the opening region were also non-uniform. Conical tapered shape of the chimney wall and presence of the opening were the main reasons for the non-uniform stress distributions [31].

Figure 6.10 shows the deformed shape of the opening region under gravity service loads. The upper and lower lintels warped towards the inside and sagged in the vertical direction. This arching action caused tensile stresses at the inner surface and compressive stresses at the outer surface of the lintels. This resulted in a gradient of vertical displacement between the mid-span and end of the lintels.

High compressive stresses occurred at the side walls of the opening region as illustrated in Figures 6.7 and 6.8. Such stress concentrations at the side edges of the opening region may lead to failure for loads that cause large lateral displacements. The ACI 307-08 code section R4.1.2.2 discusses concerns of the committee members in regards to the possibility of edge buckling of relatively thin walls through regions where tall openings are present. The full tubular cross-section in the absence of an opening maps into an I-beam with symmetric top and bottom flange areas. On the other hand, the cross-section with a large opening yields a T-beam with a single flange area. The concrete area lost in the opening region has a significant influence on the flexural capacity of the cross-section, which may lead to the high compressive stresses in the side walls of the opening.

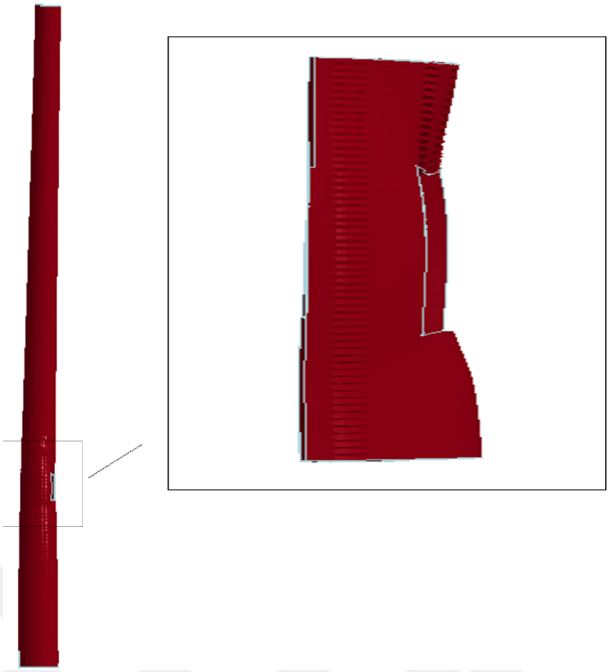

Figure 6.10. Deformed shape of the opening region under gravity service loads for both Cases 1 and 2; displacements are magnified 1000 times for illustration purposes.

Figures 6.11 and 6.12 provide the contours of axial stresses at the corner reinforcements for Case 1 and 2 under gravity service loads, respectively. The maximum tensile and compressive stresses were equal to 20 MPa for Case 1. The maximum tensile and compressive stresses were equal to 9 and 23 MPa for Case 2, respectively.

Table 6.4 summarizes the stress values of the corner reinforcements under the action of gravity service loads. The top and bottom lintels of the opening were in tension and the side walls of the opening were in compression. Therefore, the diagonal corner reinforcements were subjected to both tensile and compressive stresses. However, the vertical corner reinforcements were subjected to compressive stresses, whereas the horizontal corner reinforcements were subjected to tensile stresses.

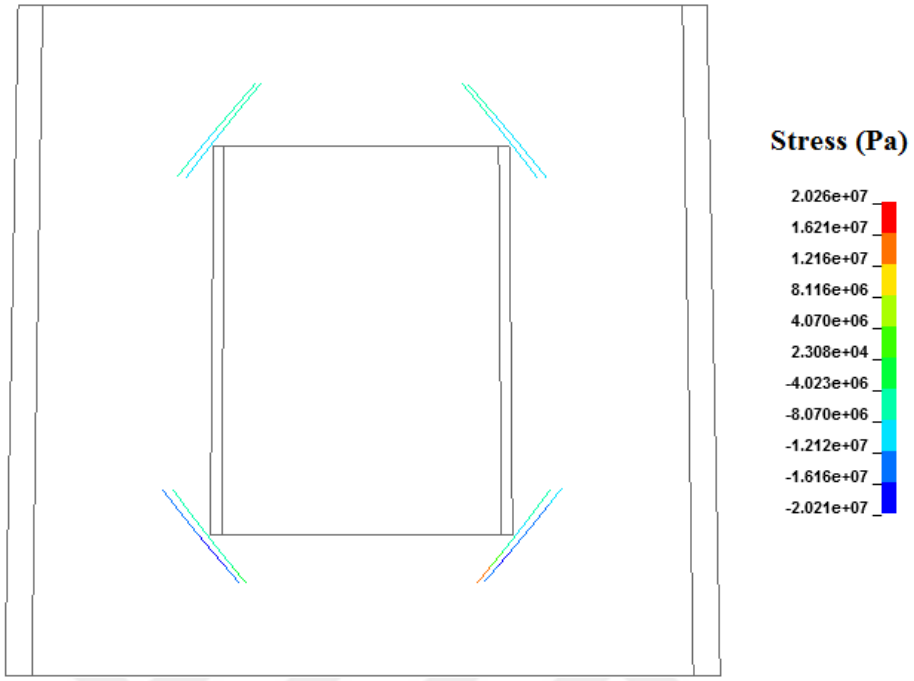

Figure 6.11. Contours of axial stresses at the diagonal corner reinforcements under gravity service loads.

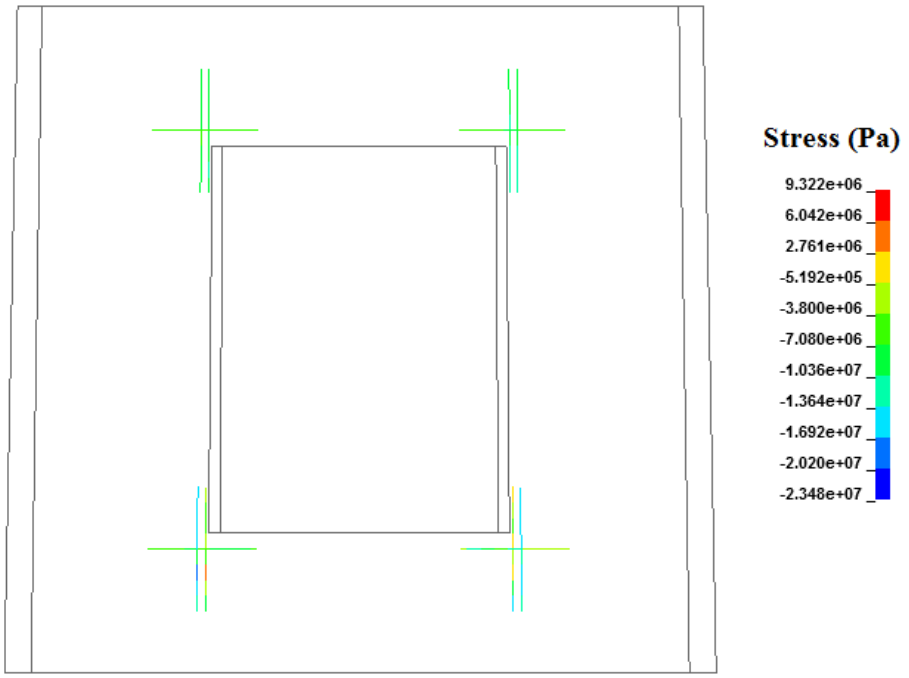

Figure 6.12. Contours of axial stresses at the vertical and horizontal corner reinforcements under gravity service loads.

Table 6.4. Stress values at the corner reinforcements under gravity service loads.

Corner Reinforcement	**Compressive Stress** (MPa)	**Tensile Stress** (MPa)	**Yield Stress** (MPa)
Diagonal	20	20	420
Horizontal & Vertical	23	9	420

Under gravity service loads, yielding did not occur at the corner reinforcements for both cases. Diagonal corner reinforcements were subjected to higher tensile stresses, however the vertical and horizontal corner reinforcements were subjected to higher compressive stresses.

Stress distributions under gravity service loads were in good agreement for both cases. Corners of the opening were subjected to compressive stresses. Moreover, no crack formations were observed under gravity service loads. Results indicated that opening region had to be subjected to tensile stresses in order to fully understand the effectiveness of the corner reinforcements. Chimney 25F-5 was further analyzed under the action of lateral service loads applied in the opposite direction of the opening.

7. SIMULATION RESULTS UNDER LATERAL SERVICE LOADS

The response of the chimney was investigated under the action of a lateral load pattern, which was in accordance with the design wind load of the chimney 25F-5. Simulations were carried out by applying lateral pressure loads on the half cylindrical surface of the windshield in the opposite direction of the opening. The brick liner and corbel rings were not included in the lateral load simulations in order to reduce the computer run-times. Simulation results were compared for two corner reinforcement design configurations in terms of crack formations and stress distributions at the opening region.

7.1. Loading Period of the Simulations

Lateral service loads were applied dynamically by using the explicit scheme of the LS-Dyna finite element code. In order to reduce the total simulation run-times, loads need to be applied within a limited period of time. Loading period of the simulations should be selected properly to obtain rapid and reliable results.

Frequency of the applied lateral loads should not coincide with the modal frequencies of the chimney to avoid the resonance, which leads to large oscillations [32]. Loading period needs to be prolonged to avoid excessive dynamic effects. However, long loading periods will result in long simulation run-times. Figure 7.1 shows the relationship between dynamic magnification factor D and the frequency ratio β. When the loading period is increased, β converges to zero and the response of the structure converges to static results.

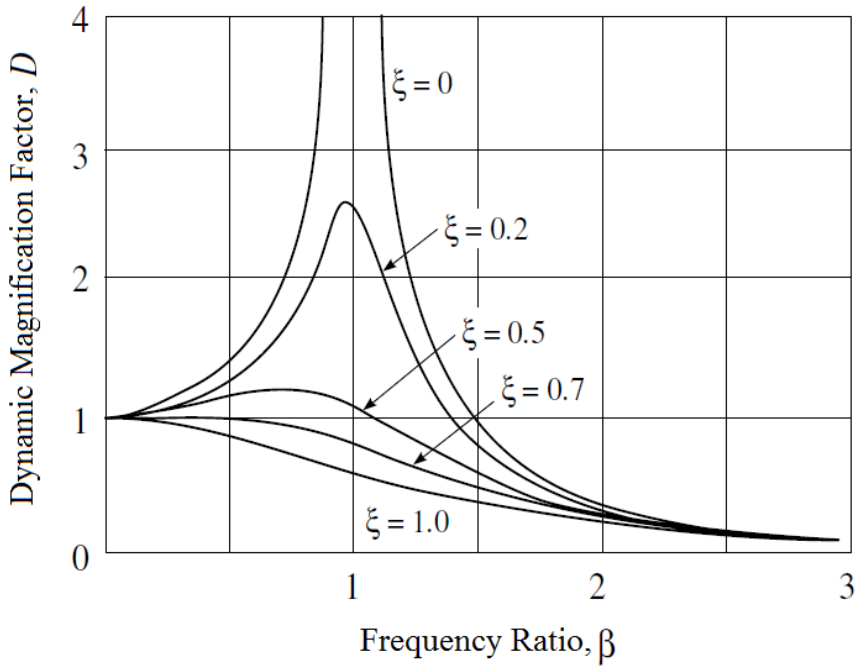

Figure 7.1. Resonance in structural dynamics [32].

Natural period of vibration of the chimney 25F-5 was eqaul to 1.65 *sec*, and the lateral pressure loads were applied dynamically within 2.5 *sec*. Therefore, frequency ratio β was equal to 0.65. Under the loading conditions, the behavior of the chimney 25F-5 will converge to the static behavior, and omit the excessive dynamic effects and oscillations.

Figure 7.2 shows the energy time-history of the chimney 25F-5 under lateral service loads. Kinetic energy during the analyses was smaller than the internal strain energy, which occurred as a result of the chimney deformations. Negligible amounts of energy were dissipated in terms of the hourglass and damping components. Total energy of the simulations was the summation of kinetic, interal, hourglass and damping energies. Total energy of simulations under lateral service loads was in the order of 3.5 MJ.

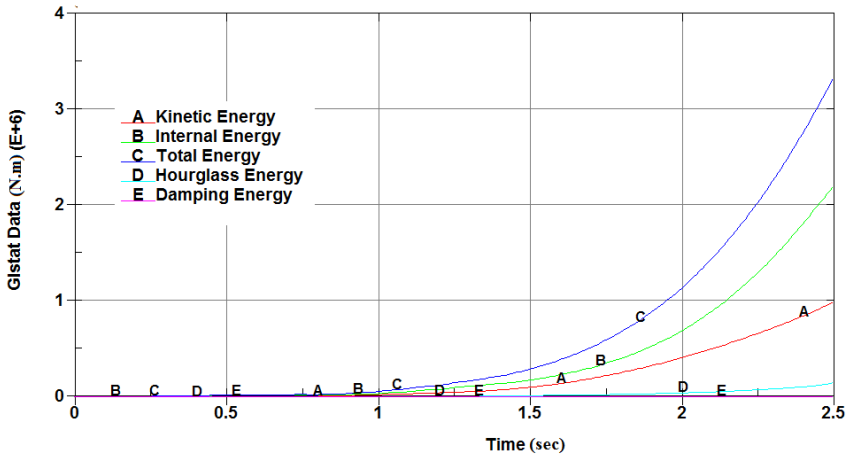

Figure 7.2. Evolution of energies under lateral service loads.

Figure 7.3 shows the relationship between top displacement and base shear of the chimney 25F-5 under lateral service loads. Small oscillations that occurred between the displacements 0.2 and 0.6 m were due to the dynamic application of the lateral service loads. Total base shear was equal to 5.5 MN, which corresponds to 22 % of the total weight of the chinney 25F-5. Top displacement was equal to 1.8 m, that correlates to a drift ratio of 1.6 %.

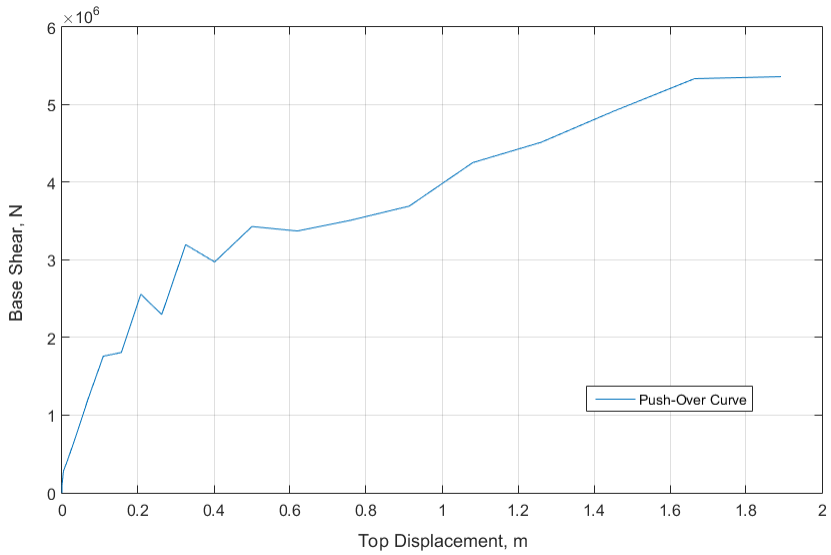

Figure 7.3. Push-over curve of the chimney 25F-5.

Figure 7.4 shows the time-history of the bending moment at the base of the chimney 25F-5 under lateral service loads. Maximum bending moment was equal to 350 $MN-m$, which corresponds to 75 % of the moment capacity at the base of the chimney 25F-5.

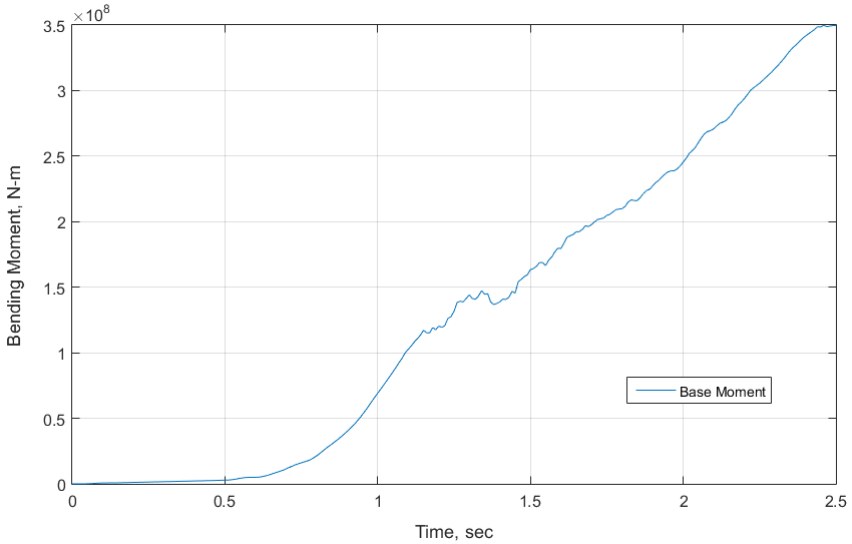

Figure 7.4. Evolution of base moment under lateral service loads.

Behavior of the chimney 25F-5 under lateral service loads was nonlinear. Simulation results were acceptable and will be further used in comparing the results of the design configurations under lateral service loads.

7.2. Comparison of Design Alternatives under Lateral Service Loads

Chimney 25F-5 was analyzed for the original design with diagonal corner rebars (Case 1) and the alternative design solution with horizontal and vertical corner rebars (Case 2) under lateral service loads. This section provides comparison of the two different corner reinforcement configurations in terms of the stress concentrations around the opening, stresses at the corner reinforcements and crack formations at the opening region.

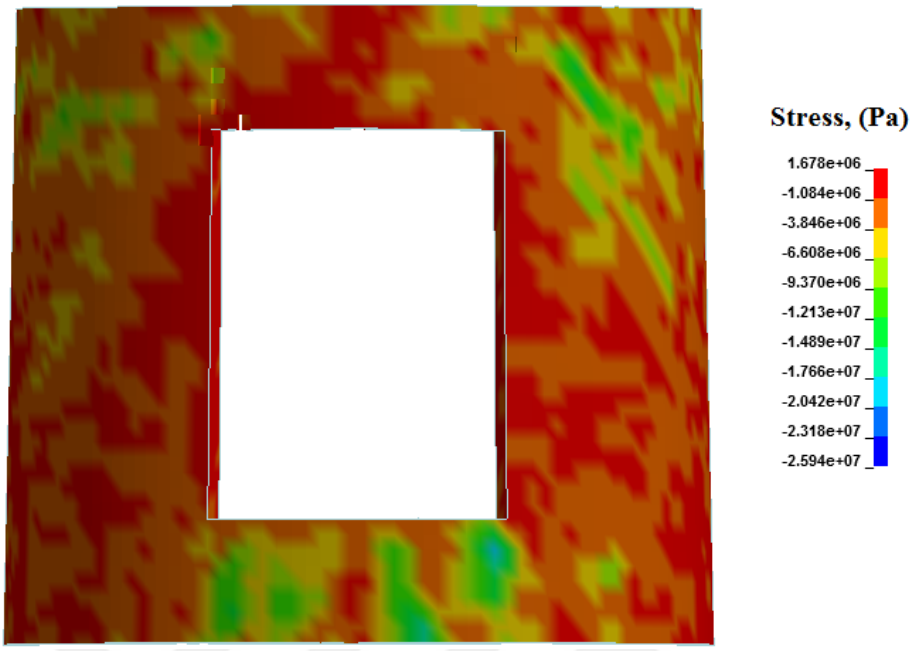

Figure 7.5. Contours of minimum principal stresses for Case 1 under lateral service loads.

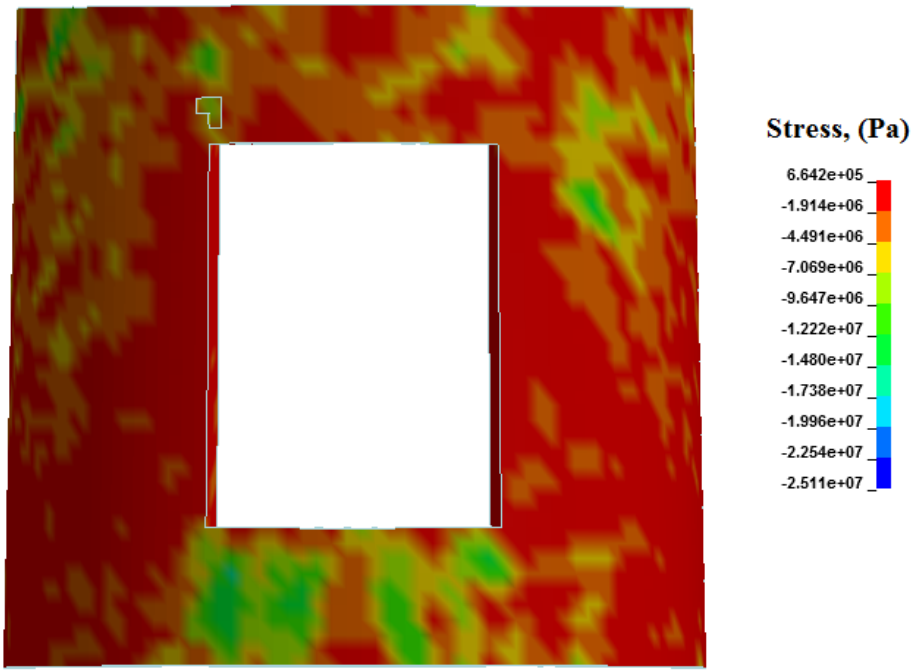

Figure 7.6. Contours of minimum principal stresses for Case 1 under lateral service loads.

Lateral service loads were applied in the opposite direction of the opening in order to obtain tensile stress concentrations at the opening region. Figures 7.5 and 7.6 show the contours of minimum principal stresses at the opening region for Case 1 and 2, respectively. Maximum tensile stresses occurred at the side walls of the opening for both Cases, which were equal to 2.5 MPa. Maximum compressive stresses occurred at the lintels of the opening for both Case 1 and 2, which were equal to 25 MPa.

Tensile stresses were developed at the side walls of the opening and compressive stresses were developed at the lintels of the opening. Under lateral loads, cross section of the chimney was not circular, it deformed into the elliptic shape in the direction of the applied loads. This resulted in concentration of compressive stresses at the lintels of the opening.

Figures 7.7 and 7.8 give the crack formations around the opening region of the chimney 25F-5 under lateral service loads for Case 1 and 2, respectively. Cracks were mainly formed at the side walls and corners of the opening, where tensile stress concentrations occurred. Minimum crack width was equal to 0.35 mm for both design methods.

Diagonal as well as vertical and horizontal corner rebars yielded close results in controlling the crack formations at the corners of the opening under lateral service loads. However, corner rebars were not effective in controlling the crack formations that occurred at the side walls of the opening.

Figures 7.9 and 7.10 provide the contours of axial stresses at the corner reinforcements for Case 1 and 2 under lateral service loads applied in the opposite direction of the opening, respectively. Corner rebars were under tensile stresses for both cases. The maximum tensile stresses were equal to 464 and 457 MPa for Case 1 and 2, respectively.

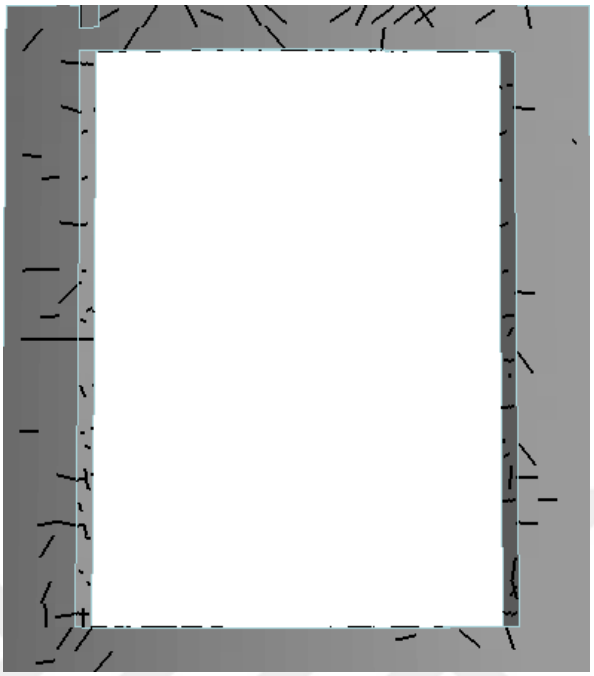

Figure 7.7. Crack formations around the opening region for Case 1 under lateral service loads.

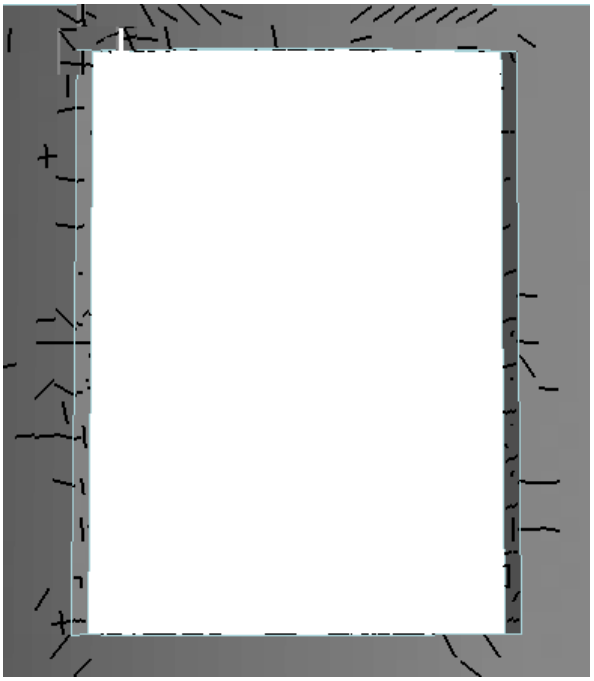

Figure 7.8. Crack formations around the opening region for Case 2 under lateral service loads.

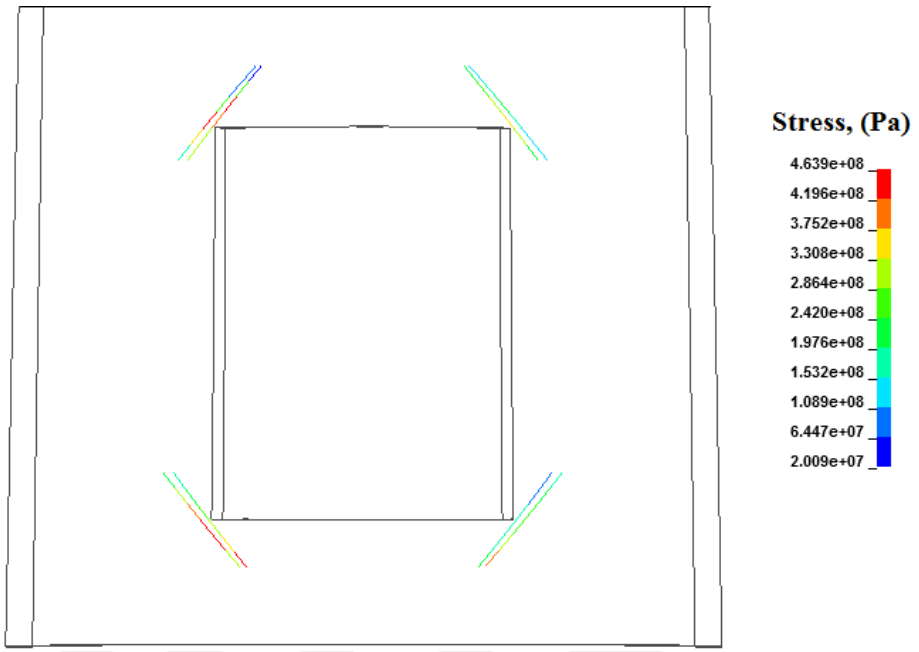

Figure 7.9. Contours of axial stresses at the diagonal corner reinforcements under lateral service loads.

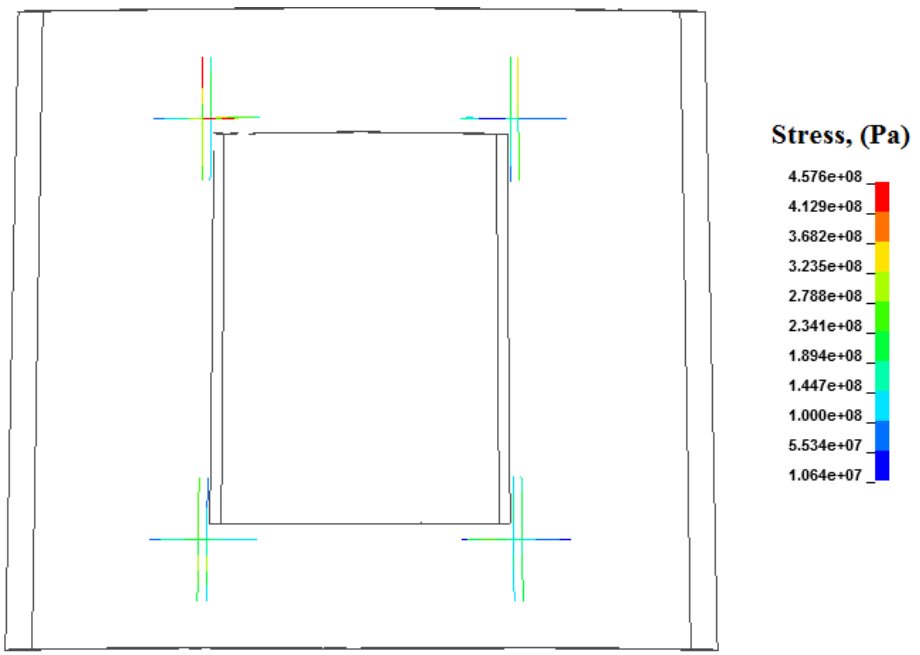

Figure 7.10. Contours of axial stresses at the vertical and horizontal corner reinforcements under lateral service loads.

Table 7.1 summarizes the stress values of the corner reinforcements under lateral service loads. Opening region was subjected to tensile forces for both smulation cases. Maximum tensile stress values were in close range for both design methods, and yielding of rebars occurred at the diagonal and vertical corner reinforcements.

Table 7.1. Stress values at the corner reinforcements under lateral service loads.

Corner Reinforcement	**Tensile Stress** (MPa)	**Yield Stress** (MPa)
Diagonal	464	420
Horizontal & Vertical	457	420

Stress distributions around the opening region as well as at the corner reinforcements were in good agreement for both cases under lateral service loads applied in the opposite direction of the opening. High tensile stresses occurred at the side walls of the opening. Moreover, crack formations were in good agreement for both design configurations.

8. CONCLUSIONS AND FUTURE WORK

8.1. Conclusions

In this study, different corner reinforcement design configurations in RC chimneys were compared under lateral and gravity service loads using full 3D FE model. FE model was generated by using hexahedral solid elements for windshield concrete and beam elements for all reinforcing steel rebars. Based on the FE analyses results, main findings are as following.

(i) Full 3D modeling provides more realistic geometry, boundary conditions and better representation of the reinforcement in RC structures. Reinforcements are included in the model explicitly, and share nodes with surrounding concrete hexahedral finite elements, simulating the behavior of reinforcing steel rebars located inside the concrete wall thickness.

(ii) Method used in the FE analysis plays crucial role in obtainig accurate and reliable results. Convergence and computation time are the main problems in nonlinear FE analysis. Most FE analysis software packages engage the implicit solution method. However, explicit time integration method implemented in LS-Dyna is better suitable for problems with high mesh resolution and nonlinearity.

(iii) Constitutive material models used in the FE analysis may affect the results of the simulations. Especially, concrete material model should be selected carefully due to its complex and nonuniform behavior. Concrete material models differ from each other in terms of defined failure or yield criterion, consideration of the tri–axial state of stress, cyclic behavior under tension and compression, compression strain softening, post–cracking response such as shear transfer after cracking or tension stiffening. Winfrith concrete material model provided adequate results under gravity and lateral service loads. Morevoer, discrete crack modeling of Winfrith concrete enabled the observation of crack formations on the concete windshield under lateral service loads.

(iv) Under gravity service loads, it was observed that lintels of the opening were in tension and subjected to both flexural and torsional moments at the both ends. Side walls of the opening were subjected to high compressive stresses. Special care needs to be taken in order to limit the deflections and loads in the lintels and side walls of the opening.

(v) Under lateral service loads, high tensile stresses were observed at the side walls of the opening. Corner reinforcements were effective in controlling the crack formations that occurred at the corners of the opening. However,they were inadequate in controlling the crack formations that mainly occurred at the side walls under lateral loads applied in the opposite direction of the opening. Special provisions and recommendations are required in terms of opening corner reinforcement configurations to reduce the crack formations at the side walls of the opening.

The results of the FE analyses indicate that the alternative design configuration consisting of horizontal and vertical corner reinforcements can be as effective as the original design configuration consisting of diagonal corner reinforcements in terms of stress distributions and crack formations under gravity and lateral service loads. The installation of the diagonal corner rebars is a difficult task in the slipform construction of RC chimneys. Therefore, it is expected that the alternative design configuration consisting of horizontal and vertical rebars will yield a practical solution for the chimney erectors.

Mechanical couplers could be used to prevent the vertical and horizontal corner rebars from relative movement. In the absence of the mechanical couplers, loads will be transferred through the concrete medium. However, by using mechanical couplers or welding of the rebars, loads will be directly transferred between the vertical and horizontal corner rebars. Moreover, the vertical and horizontal rebars to be placed at the corners could be extended along the entire span of the opening region in order to reduce crack formations and obtain better stress distributions.

8.2. Future Work

Further work is needed in order to fully understand the effects of opening corner reinforcements under cyclic loading in the opening and orthogonal directions. Contact between rebars and concrete can be implemented in order to model the effect of rebar slip, which can have effects on the crack formations under lateral loads. The current lateral load simulations did not include the brick liner and corbel rings inside the chimney. The contact or impact interaction of the brick liner with the windshield needs to be investigated under lateral loads and seismic ground motions.

REFERENCES

1. ASCE, "Minimum Design Loads for Buildings and Other Structures (ASCE/SEI 7-10)", *American Society of Civil Engineers*, 2013.

2. CICIND, "Model Code for Concrete Chimneys", *International Committee on Industrial Chimneys*, 2011.

3. ACI, "Code Requirements for Reinforced Concrete Chimneys and Commentary (ACI 307-08)", *American Concrete Institute*, 2008.

4. ACI, "Code Requirements for Reinforced Concrete Chimneys and Commentary (ACI 307-95)", *American Concrete Institute*, 1995.

5. ACI, "Code Requirements for Reinforced Concrete Chimneys and Commentary (ACI 307-98)", *American Concrete Institute*, 1998.

6. ACI, "Proposed Standard Specification for the Design and Construction of Reinforced Concrete Chimneys (ACI 505-53)", *American Concrete Institute*, 1953.

7. ACI, "Proposed Standard Specification for the Design and Construction of Reinforced Concrete Chimneys (ACI 505-54)", *American Concrete Institute*, 1954.

8. Mingle, J., "Design of Reinforced Concrete Chimneys", *ACI Journal Proceedings*, Vol. 14, 1918.

9. ACI, "Building Code Requirements for Structural Concrete and Commentary (ACI 318-11)", *American Concrete Institute*, 2011.

10. ISE, "Standard Method of Detailing Structural Concrete", *The Structural Engineer*, 2006.

11. Lin, C. and C. Kuo, "Behavior of Shear Wall with Opening", *9th World Conference*

on Earthquake Engineering, 1988.

12. CIM, "Bar Detailing at Wall Openings", *American Concrete Institute*, 2010.

13. Daniel, J., K. Shiu and W. Corley, "Openings in Earthquake-Resistant Structural Walls", *Journal of Structural Engineering, ASCE*, pp. 1660–1676, 1986.

14. Boon, K., A. Diah and L. Loon, "Flexural Behavior of Reinforced Concrete Slab with Opening", *MUCET, Malaysian Technical Universities Conference on Engineering and Technology*, 2009.

15. Mansur, M., K. Tan and S. Lee, "Design Method for Reinforced Concrete Beams with Large Openings", *ACI Structural Journal*, pp. 517–524, 1985.

16. ACI, "Code Requirements for Reinforced Concrete Chimneys and Commentary (ACI 307-69)", *American Concrete Institute*, 1969.

17. Kilic, S. and M. Sozen, "Evaluation of Effect of August 17, 1999, Marmara Earthquake on Two Tall reinforced Concrete Chimneys", *ACI Structural Journal*, pp. 357–364, 2003.

18. Hallquist, J., *LS-Dyna Theoretical Manual*, Livermore Software Technology Corporation, Livermore, California, 2006.

19. Kilic, S., F. Saied and A. Sameh, "Efficient Iterative Solvers for Structural Dynamics Problems", *Computers & Structures*, pp. 2363–2375, 2004.

20. Belytschko, T., W. Liu, B.Moran and K. Elkhodary, *Nonlinear Finite Elements for Continua and Structures*, John Wiley & Sons, Inc., West Sussex, United Kingdom, 2014.

21. Bathe, K., *Finite Element Procedures*, Prentice Hall, New Jersey, NJ, USA, 1996.

22. Chen, W., *Plasticity in Reinforced Concrete*, McGrow Hill, NY, USA, 1982.

23. Schwer, L., *An Introduction to the Winfrith Concrete Model*, Schwer Engineering & Consulting Services, Windsor, California, 2010.

24. Broadhouse, B., *The Winfrith Concrete Model in LS-Dyna3D*, AEA Technology, Dorchester, United Kingdom, 1995.

25. Ottosen, N., "A Failure Criterion for Concrete", *Journal of the Engineering Mechanics Division, ASCE*, pp. 528–535, 1977.

26. Wilson, J. and S. Kilic, "Experimental Study to Investigate the Cyclic Behavior of Reinforced Concrete Chimney Sections with Openings", *CICIND Report*, Vol. 19(2), pp. 9–24, 2003.

27. Kilic, S. and S. Altay, "Simulation of the Cyclic Hysteretic Response of Reinforced Concrete Chimneys", *ICCT International Conference on Industrial Chimneys & Cooling Towers*, pp. 271–277, 2014.

28. Altay, S., *Experimental Investigation and 3D Cyclic Finite Element Simulation of RC Exterior Beam-Column Joint*, Ph.D. Thesis, Bogazici University, 2010.

29. Roger, R., *TrueGrid User's Manual*, XYZ Scientific Applications Inc., Pleasant Hill, California, 2014.

30. Kilic, S., S. Altay and D. Akyniyazov, "Finite Element Meshing Techniques for Modeling RC Chimneys", *CICIND Report*, Vol. 32(1), pp. 67–70, 2016.

31. Kilic, S., D. Akyniyazov and S. Altay, "Additional Reinforcements and the Response of RC Chimneys with Large Openings", *CICIND Report*, Vol. 32(2), pp. 149–152, 2016.

32. Clough, R. and J.Penzien, *Dynamics of Structures*, Computers & Structures, Inc., Berkeley, California, 2003.